Quaternary Science Reviews 282 (2022) 107456

Contents lists available at ScienceDirect

Quaternary Science Reviews

journal homepage: www.elsevier.com/locate/quascirev

The late Holocene history of Lake Cahuilla: Two thousand years of repeated fillings within the Salton Trough, Imperial Valley, California

Thomas K. Rockwell [a, *], Aron J. Meltzner [b, c], Erik C. Haaker [d], Danielle Madugo [e]

[a] Dept. Geological Sciences, San Diego State University, San Diego, CA, 92182, USA
[b] Earth Observatory of Singapore, Nanyang Technological University, 639798, Singapore
[c] Asian School of the Environment, Nanyang Technological University, 639798, Singapore
[d] G3Soilworks, Inc., 350 Fischer Avenue, Costa Mesa, CA, 92626, USA
[e] Garrick Institute for the Risk Sciences, University of California Los Angeles, Engineering VI, Phase 1, 404 Westwood Plaza, Los Angeles, CA, 90095, USA

ARTICLE INFO

Article history:
Received 11 November 2021
Received in revised form
26 February 2022
Accepted 6 March 2022
Available online xxx

Handling Editor: Dr I Hendy

Keywords:
Lake Cahuilla
Lake chronology
Radiocarbon
Paleoseismology
Archaeology

ABSTRACT

To constrain the timing of the past seven lake highstands in the Salton Trough, we compiled 423 radiocarbon dates, of which 284 are reliable and have good stratigraphic control, from paleoseismic and archeological sites in the basin. We developed two OxCal models that assume most charcoal, wood, seeds, and twigs recovered from organic mats at or near the shoreline are derived from material that grew within the lake footprint, and therefore date a dry period between lakes. Charcoal samples collected from lacustrine clastic strata may have also been derived from fires burned during a dry period. As an initial constraint, we assume that samples older than those in earlier lake deposits have age inheritance. Assuming the dates are accurately described by their respective 2σ uncertainties, we ran all dates that would run in a preliminary OxCal model, and then removed those with a poor agreement index as defined in OxCal. From this, of the 423 total dates in the compilation, 151 dates are used in the base model and 149 dates are used in an alternative model, with the differences in the models resulting from choices of whether to include or exclude specific dates that may or may not be representative of a particular dry period between lakes. Where the two models agree, the results are robust, but where the models differ, any differences are taken as uncertainty in the lake ages. Historical accounts and a high-resolution paleohydrologic reconstruction allow us to refine some lake ages.

The age windows for the past seven Lake Cahuilla highstands are 1731–1733 CE (Lake A), 1618–1636 CE (Lake B), 1486–1503 CE (Lake C), 1118–1165 or 1192–1241 CE (Lake D), 1007–1070 CE (Lake E), 930–966 CE (Lake F), and 612–5 BCE (Lake G). These ages represent the maximum allowable ranges during which a lake may have filled the basin up to the +13 m highstand elevation; the basin may have been dry for significant portions of each time window, though the lake filling and desiccation episodes may have extended beyond the stated highstand age range for each lake. If the paleohydrologic constraints are ignored, some of the lakes may have initiated earlier, by up to three decades. Additional dates would be needed to further bracket the ages of the earlier lakes. Notably, 120 of the original 284 reliable dates were rejected because they clearly violate stratigraphic ordering, implying that more than 40% of all radiocarbon dates in the Salton Basin exhibit statistically significant age inheritance.

1. Introduction

Lake Cahuilla was a freshwater lake that filled the Salton Trough in southeastern California many times during the Holocene, up to the sill elevation at ~13 m above sea level (Sykes, 1937; Wilke, 1978; Waters, 1983; Philibosian et al., 2011). Each filling of Lake Cahuilla followed an avulsion of the Colorado River (Waters, 1983; Li et al., 2008), away from its usual southerly course to the Gulf of California, with flow instead directed west and north along the Alamo and New Rivers (Fig. 1). Six filling episodes resulting in full lakes have been recognized in the past ~1100 years, all of them from before written history in the Salton Basin, although there are oral Indigenous American accounts that record the latest filling (Modesto and

* Corresponding author.
E-mail addresses: trockwell@sdsu.edu (T.K. Rockwell), meltzner@ntu.edu.sg (A.J. Meltzner), ehaaker@g3soilworks.com (E.C. Haaker), daniellemadugo@gmail.com (D. Madugo).

https://doi.org/10.1016/j.quascirev.2022.107456

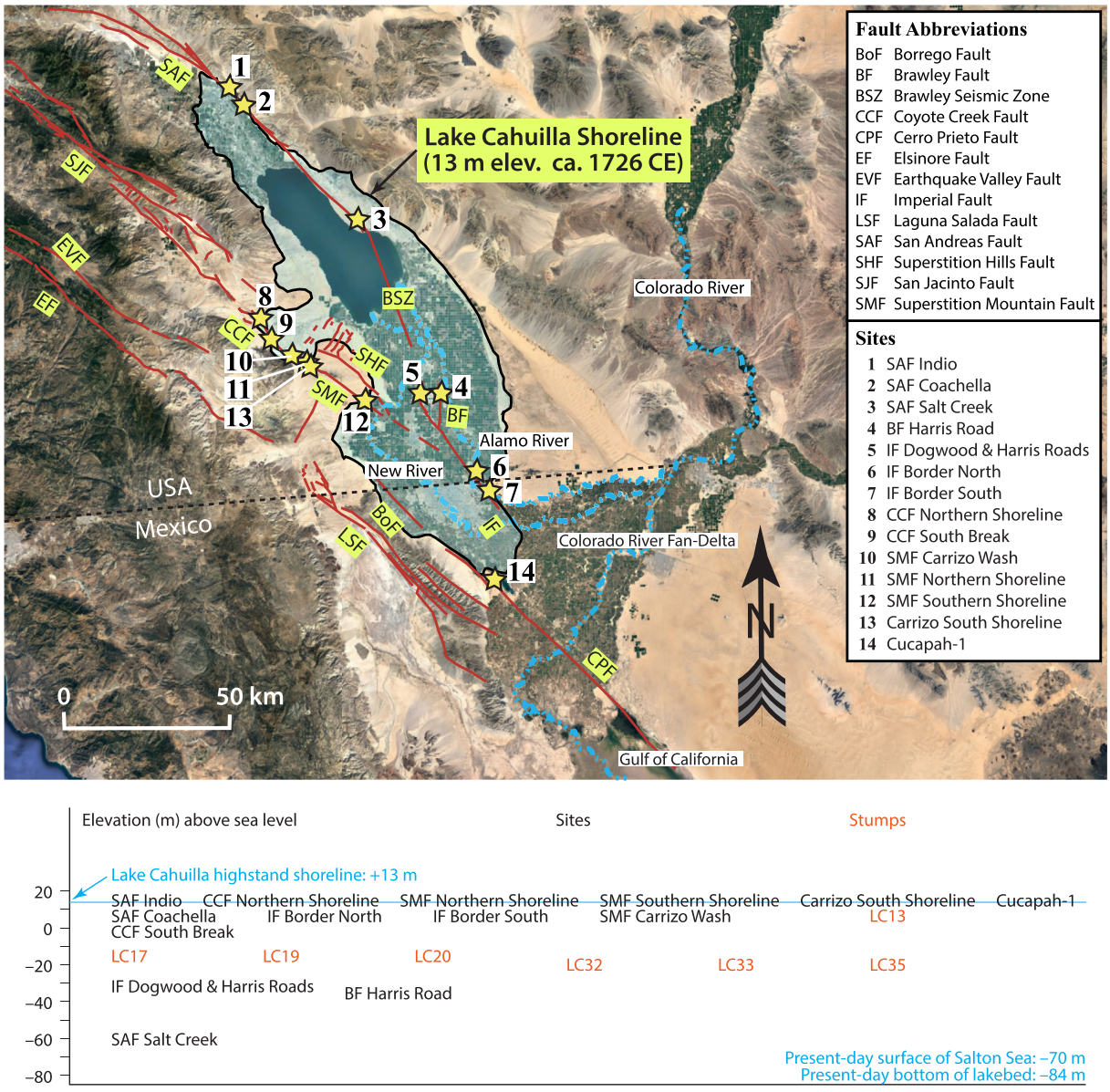

Fig. 1. *Top:* Map of the shoreline and inundation zone of Lake Cahuilla, outlined in black. Colorado River channels (including the Alamo and New Rivers) are marked as light blue dash-dotted lines. Faults (in red) are adapted from Fletcher et al. (2014), Rockwell et al. (2015), and U.S. Geological Survey and California Geological Survey (2020). Referenced sites are indicated by stars, with site names listed to the right. Stratigraphic descriptions and context of radiocarbon samples for sites 2 and 4–13 are provided in Supplementary Text S1 and Supplementary Figs. S1–S20 and were compiled from the following. Site 2: Philibosian et al. (2011); Site 4: Meltzner et al. (2006); Site 5: Meltzner (2006), Rockwell et al. (2011); Site 6: Jerrett (2015), Wessel (2015); Site 7: Thomas and Rockwell (1996); Site 8: Pollard and Rockwell (1995); Site 9: Orgil (2001); Site 10: Ragona, 2003, Verdugo (2004); Site 11: Gurrola and Rockwell (1996); Site 12: Faneros (2005); Site 13: White (2017). For Site 1 see Sieh (1986) and Sieh and Williams (1990); for Site 3 see Williams (1989) and Sieh and Williams (1990). Details for Site 14 are in Supplementary Table S1. *Bottom:* Sites (black text) arranged by elevation, along with the Lake Cahuilla highstand shoreline and lake bottom (blue text). Also shown are elevations of the mesquite stumps used in our model (red text; Rockwell et al., 2018). All elevations given relative to present mean sea level. (For interpretation of the references to colour in this figure legend, the reader is referred to the Web version of this article.)

Mount, 1980). The lake almost filled from an avulsion of the main channel in 1905 CE (Ross, 2020), which resulted in two years of flooding into the Salton depression; the Salton Sea is a remnant of that flooding episode (Cory, 1913; Sykes, 1937) and persists due to irrigation run-off and leakage from unlined canals.

Resolving the precise timing of these past lakes is important from several perspectives. For one, the shorelines of the lakes were occupied by the Cahuilla and Kumeyaay Indigenous Americans (Laylander, 1997, and references therein), so a precise lake chronology provides a temporal framework to interpret past occupation events. Archeological sites are also found below the highstand shoreline of Lake Cahuilla, and the precise lake timing is relevant for these occupations as well.

Another motivation is that the lake paleo-shoreline crosses several major faults of the southern San Andreas fault system, which means that the lake sediments are an archive of the rupture history of much of the southern San Andreas system (Rockwell et al., 2018). Many of the faults have been studied at paleoseismic sites developed in the lacustrine deposits, but precise dating of the past earthquakes has been hampered in many of these studies by age inheritance in detrital charcoal. That is, the radiocarbon date on a piece of detrital charcoal dates to the time of wood growth and death and not the timing of the lake or deposit that hosts the charcoal. Further, most charcoal samples collected from lake

deposits must have originated either from outside the lake or from wood that grew in the lake footprint prior to inundation, as most wood does not grow under water, and wood does not burn underwater; these different possible origins lead to potentially clashing implications for each sample as they can pre-date or be equivalent to the age of any lake. Rockwell et al. (2018) avoided this ambiguity by dating in situ stumps that had been drowned by the most recent two highstands of the lake, but no in situ stumps have been found to date the earlier late Holocene lakes.

A precise lake chronology would allow a sequencing of earthquakes that overcomes the chronological limitations at individual sites, particularly sites where most samples have significant age inheritance. Paleoseismic records have been documented at sites that range from at or near the shoreline (+13 m: Sieh, 1986; Gurrola and Rockwell, 1996; Philibosian et al., 2011) to as low as 60 m below sea level (Sieh and Williams, 1990; Williams and Seitz, 2005, 2006; Rockwell et al., 2011), or imaged below the lake bottom (Brothers et al., 2009, 2011), and all sites have exposed multiple late Holocene lake phases.

Other applications of a precise lake chronology include studies of the Colorado River delta, an extensive fan delta system that is now host to extensive agriculture both north and south of the international border, as well as Baja California's capital and largest city, Mexicali. Knowing when water flowed north into the Salton Trough versus south to the Gulf provides information on the architecture of the delta.

The timing of the most recent Lake Cahuilla highstand ("Lake A″) has been well constrained by Rockwell et al. (2018) at CE 1726 ± 7 (2σ), based primarily on paired dates from in situ stumps that grew within the Lake Cahuilla footprint during the dry period prior to the most recent highstand, combined with early historical accounts. The timing of the penultimate lake highstand ("Lake B″) was moderately constrained at CE 1577 ± 67 (2σ), based on the aforementioned dates and a small selection of additional samples recovered from within Lake B and earlier deposits (Rockwell et al., 2018).

In this study, we build upon the model developed for the past two full lake inundations by Rockwell et al. (2018) by compiling and analyzing 423 radiocarbon dates from sites within the Lake Cahuilla footprint (Fig. 1; Supplementary Table S1). From this database, we develop a base model of the ages of lakes and intervening dry periods that is consistent with the data from the various sites within the lake. Using OxCal (Bronk Ramsey, 2008, 2009a) and the most recent radiocarbon calibration curve (IntCal20; Reimer et al., 2020), we extend the model back to include the past seven Lake Cahuilla highstands. In addition, we reorganize the structure of the OxCal model of Rockwell et al. (2018) to refine the ages of the past two highstands. We compare this model to the paleoclimate record of the Colorado Plateau region and inferred Colorado River flow (Meko et al., 2007; Robeson et al., 2020), which is the source region for >90% of the water that filled the various lake episodes (Rockwell et al., 2018). We then discuss how eliminating or adding a few dates, which may be outliers, affects the stability of the base model.

2. Prior work

2.1. Lake Cahuilla reconstructions: early efforts

Prior work to establish the chronology of lake highstands was undertaken by Wilke (1978), Waters (1983), Gurrola and Rockwell (1996), and Philibosian et al. (2011). Wilke (1978) focused on the late prehistoric human ecology at Lake Cahuilla. He applied ^{14}C dating on various cultural elements to establish that water had been in the basin, possibly intermittently, since about 900 CE, although all of his dates have large uncertainties of 100–200 years and are thus of limited use. Waters (1983) focused specifically on the history of highstands of Lake Cahuilla, but identified only four highstand episodes in the past 2 ka, and again, had large uncertainties associated with his ^{14}C dates. Gurrola and Rockwell (1996) worked at a site where the Superstition Mountain fault crosses the shoreline. They recognized 5 or 6 highstands and applied higher resolution ^{14}C dating to establish a chronology of these lakes. Philibosian et al. (2011), in contrast, recognized evidence for up to seven lakes at the Coachella paleoseismic site located at a few meters below the shoreline, although their lowest potential lake sequence had limited exposure, and therefore its interpretation is equivocal (Supplementary Text S1). They applied much higher resolution ^{14}C dates than in most prior work and we use most of these in our study. Nonetheless, each of these earlier studies was based on the limited number of dates available to the authors of those studies; there is significant room for improvement of the chronology from each of these earlier studies, which could be obtained by combining dates collected in recent decades from all the sites within the basin.

2.2. Stump dates and ages of the past two lakes

The most recent effort to refine the Lake Cahuilla chronology was undertaken by Rockwell et al. (2018), who dated stumps drowned by the past two lake inundations. Based on their new dates and analysis of historical constraints, they place the timing of the most recent full lake (Lake A) at CE 1726 ± 7 (2σ). This age accounts for three things: the stump ages that force the timing of the highstand into the 18th century; the written accounts by Kino that indicate that the Colorado River was flowing to the Gulf of California as late as 1706; and the lack of description of water in the basin when Anza's expedition traversed the region in 1774. The penultimate lake (Lake B) had a larger uncertainty of CE 1577 ± 67 (2σ) for two reasons: first, the age was based only on radiocarbon data with no historical constraints; and second, there is a bimodal probability distribution or double peak in the calibration curve for that time period, which tends to inhibit a narrow calibrated age window. Rockwell et al. (2018) did not attempt to refine the age estimates for any lakes prior to Lake B. In this paper, we build upon the work of Rockwell et al. (2018) by adding additional dates from Lake B strata, plus many more from older stratigraphy, spanning five older lakes (Lakes C, D, E, F, and G) (Table 1).

3. Methods

3.1. Depositional environments for radiocarbon samples

Apart from stumps in growth position, which will be discussed in the next section, samples were collected from one of seven depositional environments, each of which has specific implications for the interpretation.

Samples recovered from within laminated or thinly bedded silty and clayey units, interpreted as lacustrine deposits, are derived either from the desert floor below the shoreline (and incorporated into the lake strata during flooding of the basin) or from outside the lake. In Table 1, samples collected from lake strata are indicated as "La".

Some localities describe sediments interpreted as delta deposits, indicated in Table 1 as "De", which represent deposition during flooding of the Salton depression (e.g., Jerrett, 2015; Wessel, 2015). These strata are typically dominated by silt and sandy silt and are

Table 1
Sample details and stratigraphic context for modeled radiocarbon dates.

Lab Code *	Lab Sample #	Sample Name	Stratigraphic Unit	Depositional Environment **	Material	^{14}C age yr	± yr	Model 1 ***	Model 2 ***	OxCal Function	Site	Ref ****	Elevation m *****
Maximum age of dry period after Lake A (includes dates from post-Lake A desiccation)													
CAMS-LLNL	90755	BFH-C-25	130	Bu	charcoal	65	40	Include	Include	After	Brawley Harris Rd	M06	−36.5
CAMS-LLNL	90753	BFH-C-33	154–156	Fl or De	charcoal	70	40	Include	Include	After	Brawley Harris Rd	M06	−36.5
CAMS-LLNL	90756	BFH-C-30	130	Bu	charcoal	70	40	Include	Include	After	Brawley Harris Rd	M06	−36.5
CAMS-LLNL	90754	BFH-C-24	130	Bu	charcoal	80	30	Include	Include	After	Brawley Harris Rd	M06	−36.5
CAMS-LLNL	97476	SMF-S18	Q1	Fl	charcoal	85	40	Include	Include	After	SMF South Shoreline	F05	13
CAMS-LLNL	90752	BFH-C-29	156	Fl or De	charcoal	105	40	Include	Include	After	Brawley Harris Rd	M06	−36.5
CAMS-LLNL	97484	SMF-S38	Q1	Fl	charcoal	130	40	Include	Include	After	SMF South Shoreline	F05	13
		2382001-1	200	Ae	charcoal	230	50	Include	Include	After	SMF Carrizo Wash	R03	8
Maximum age of Lake A (burns from sites at the shoreline; wood could be derived from above or at shoreline)													
Beta	78082	CCF-T1-C3		Sh	charcoal	0	80	Include	Include	After	CCF North Shoreline	P95	13
Beta	37907	RIV-1182a		Cu	charcoal	50	60	Include	Include	After	RIV-1182	L97a	12.2
Beta	37906	RIV-1182b		Cu	charcoal	80	50	Include	Include	After	RIV-1182	L97a	12.2
Beta	57861	RIV-1349a		Cu	charcoal	80	70	Include	Include	After	RIV-1349	L97c	12.2
Beta	57860	RIV-1349b		Cu	charcoal	110	80	Include	Include	After	RIV-1349	L97c	12.2
Beta	37904	RIV-3682a			charcoal	210	50	Include	Include	After	RIV-3682	L97d	12.2
		IMP-5296		Cu	charcoal	220	70	Include	Include	After	IMP-5296	L97b	12.2
Beta	37911	RIV-3144a			charcoal	300	50	Include	Include	After	RIV-3144	L97a	12.2
Beta	37902	RIV-3682b			charcoal	320	60	Include	Include	After	RIV-3682	L97d	12.2
Beta	57863	RIV-1331		Cu	charcoal	320	90	Include	Include	After	RIV-1331	L97c	12.2
Dry period before Lake A or Maximum age of Lake A													
CAMS-LLNL	125189	Nb1m57A-b-hum	1La	La	humic	−5	30	Include	Include	Phase	SAF Coachella	P11	9
CAMS-LLNL	97478	SMF-S21	Q2	Sh	organic mat	80	40	Include	Include	Phase	SMF South Shoreline	F05	13
UCIAMS	157516	CSS-1P-twig		Sh	charcoalized twig in org. mat	90	40	Include	Include	Phase	Carrizo South Shoreline	W17	13
UCIAMS	35630	Nb1m22A-c	1Lb	La	charcoal	105	20	Include	Include	Phase	SAF Coachella	P11	9
UCIAMS	35404	Nb1m45A-c	1S	Ae (or Sh)	charcoal	125	20	Include	Include	Phase	SAF Coachella	P11	9
UCIAMS	47182	IFD-T2-C61a	240 (?)	Fl or La	charcoal	130	15	Include	Include	Phase	Imperial Dogwood Rd	R11	−32
UCIAMS	157512	CSS-1P-2w		Sh	wood from organic mat	145	15	Include	Include	Phase	Carrizo South Shoreline	W17	13
UCIAMS	157518	CSS-8P-1		Sh	charcoal from organic mat	150	20	Include	Include	Phase	Carrizo South Shoreline	W17	13
UCIAMS	55811	IFD-T2-C61b	240 (?)	Fl or La	charcoal	155	20	Include	Include	Phase	Imperial Dogwood Rd	R11	−32
QL	4647	C28	P1	Sh	bulk date on organic mat	159	14	Include	Include	Phase	SMF North Shoreline	G96	13
UCIAMS	157522	CSS-9P-1		Sh	charcoal from organic mat	160	60	Include	Include	Phase	Carrizo South Shoreline	W17	13
UCIAMS	35405	Nb1m51A-c	1S	Ae (or Sh)	charcoal	175	15	Include	Include	Phase	SAF Coachella	P11	9
QL	4648	C47	P1	Sh	bulk date on organic mat	177	14	Include	Include	Phase	SMF North Shoreline	G96	13
UCIAMS	157513	CSS-1P-2c		Sh	charcoal from organic mat	180	20	Include	Include	Phase	Carrizo South Shoreline	W17	13
UCIAMS	157520	CSS-8P-3		Sh	charcoal from organic mat	180	20	Include	Include	Phase	Carrizo South Shoreline	W17	13
UCIAMS	157521	CSS-8P-4		Sh	charcoal from organic mat	180	25	Include	Include	Phase	Carrizo South Shoreline	W17	13
QL	4649	C18	P2	Sh	bulk date on organic mat	190	90	Include	Include	Phase	SMF North Shoreline	G96	13
QL	643	CAH-80-4		La	organic mat	192	50	Include	Include	Phase	SAF Indio	S90	13
UCIAMS	157519	CSS-8P-2		Sh	charcoal from organic mat	195	20	Include	Include	Phase	Carrizo South Shoreline	W17	13
CAMS-LLNL	125108	Nb1m57A-b-AAA	1La	La	AAA	200	35	Include	Include	Phase	SAF Coachella	P11	9
UCIAMS	35408	Sb1m44A-c	1S	Ae (or Sh)	charcoal	210	15	Include	Include	Phase	SAF Coachella	P11	9
UCIAMS	157515	CSS-1P-3c		Sh	charcoal from organic mat	220	25	Include	Include	Phase	Carrizo South Shoreline	W17	13

Table 1 (*continued*)

Lab Code *	Lab Sample #	Sample Name	Stratigraphic Unit	Depositional Environment **	Material	^{14}C age yr	± yr	Model 1 ***	Model 2 ***	OxCal Function	Site	Ref ****	Elevation m *****
UCIAMS	157517	CSS-1P-seeds		Sh	seeds from organic mat	230	25	Include	Include	Phase	Carrizo South Shoreline	W17	13
QL	4654	P2b	P2	Sh	bulk date on organic mat	230	40	Include	Include	Phase	SMF North Shoreline	G96	13
QL	642	CAH-80-3		La	organic mat	231	45	Include	Include	Phase	SAF Indio	S90	13
AA	33526	SB 14C-117	C1	La	charcoal	235	60	Include	Include	Phase	CCF South Break	O01	−4
AA	33524	SB 14C-107	C1	La	charcoal	250	55	Include	Include	Phase	CCF South Break	O01	−4
UCIAMS	155645	IFBT2-127	220–270	Fl or De	charcoal	255	15	Include	Include	Phase	Imperial Border North	J15	8
CAMS-LLNL	125109	Nb1m57A-c	1La	La	charcoal	260	40	Include	Include	Phase	SAF Coachella	P11	9
UCIAMS	157523	CSS-9P-2		Sh	charcoal from organic mat	265	25	Include	Include	Phase	Carrizo South Shoreline	W17	13
UCIAMS	155637	IFBT1-47	200	La	charcoal	275	20	Include	Include	Phase	Imperial Border North	W15	8
UCIAMS	157525	CSS-6		Sh	charcoal	280	25	Include	Include	Phase	Carrizo South Shoreline	W17	13
UCIAMS	157524	CSS-3		Sh	charcoal	290	20	Include	Include	Phase	Carrizo South Shoreline	W17	13
UCIAMS	155649	IFBT2-141	220	De	charcoal	310	15	Include	Include	Phase	Imperial Border North	J15	8
AA	33525	SB 14C-115	C1	La	charcoal	350	55	Include	Include	Phase	CCF South Break	O01	−4
UCIAMS	111439	LC32 outer		–	in situ stump below Lake A	70	20	Include	Include	Sequence		H12	−20
UCIAMS	111438	LC32 inner		–	in situ stump below Lake A	215	20	Include	Include	Sequence		H12	−20
UCIAMS	111435	LC17 outer		–	in situ stump below Lake A	115	20	Include	Include	Sequence		H12	−16
UCIAMS	101759	LC17 inner		–	in situ stump below Lake A	130	15	Include	Include	Sequence		H12	−16
UCIAMS	111436	LC19 outer		–	in situ stump below Lake A	115	20	Include	Include	Sequence		H12	−15
UCIAMS	101761	LC19 inner		–	in situ stump below Lake A	205	15	Include	Include	Sequence		H12	−15
UCIAMS	111441	LC33 outer		–	in situ stump below Lake A	125	20	Include	Include	Sequence		H12	−20
UCIAMS	111440	LC33 inner		–	in situ stump below Lake A	125	20	Include	Include	Sequence		H12	−20
UCIAMS	111443	LC35 outer		–	in situ stump below Lake A	125	20	Include	Include	Sequence		H12	−20
UCIAMS	111442	LC35 inner		–	in situ stump below Lake A	205	15	Include	Include	Sequence		H12	−20
UCIAMS	111437	LC20 outer		–	in situ stump below Lake A	155	20	Include	Include	Sequence		H12	−15
UCIAMS	101762	LC20 inner		–	in situ stump below Lake A	160	15	Include	Include	Sequence		H12	−15
UCIAMS	111434	LC13 outer		–	in situ stump below Lake A	180	20	Include	Include	Sequence		H12	8
UCIAMS	101757	LC13 inner		–	in situ stump below Lake A	180	15	Include	Include	Sequence		H12	8
Dry period before Lake B or Maximum age of Lake B													
UCIAMS	155639	IFBT2-109	361	De	charcoal	230	170	Include	Include	Phase	Imperial Border North	J15	8
UCIAMS	35427	Sb3m45A-c	2Ld	La	charcoal	310	15	Include	Include	Phase	SAF Coachella	P11	9
QL	4651	C25b	P3	Sh	charcoal from organic mat	310	40	Include	Include	Phase	SMF North Shoreline	G96	13
UCIAMS	48820	IFD-T2-C67	306	La	charcoal	320	15	Include	Include	Phase	Imperial Dogwood Rd	R11	−32
UCIAMS	155615	IFBT1-15	355	De	charcoal	330	15	Include	Include	Phase	Imperial Border North	W15	8
UCIAMS	35412	Sb2m10A-c	2Ld	La	charcoal	335	15	Include	Include	Phase	SAF Coachella	P11	9
UCIAMS	35426	Sb3m44A-c	2Ld	La	charcoal	335	20	Include	Include	Phase	SAF Coachella	P11	9
UCIAMS	183592	SB 3DIII-23B	C3	–	in situ bush below Lake B	350	15	Include	Include	Phase	CCF South Break	O01	−4
CAMS-LLNL	73117	SB 3DIII-23A	C3	–	in situ bush below Lake B	350	40	Include	Include	Phase	CCF South Break	O01	−4
UCIAMS	35413	Sb2m10B-c	2Ld	La	charcoal	360	25	Include	Include	Phase	SAF Coachella	P11	9
UCIAMS	35428	Sb3m48A-c	2Ld	La	charcoal	380	15	Include	Include	Phase	SAF Coachella	P11	9
CAMS-LLNL	128364	Sb2m26A-c	2Lb	La	charcoal	385	35	Include	Include	Phase	SAF Coachella	P11	9
CAMS-LLNL	97482	SMF-S29	Q3	Sh	charcoal	395	40	Include	Include	Phase	SMF South Shoreline	F05	13
CAMS-LLNL	128363	Nb2m36A-c	2Lb	La	charcoal	400	30	Include	Include	Phase	SAF Coachella	P11	9

(*continued on next page*)

Table 1 (*continued*)

Lab Code *	Lab Sample #	Sample Name	Stratigraphic Unit	Depositional Environment **	Material	^{14}C age yr	± yr	Model 1 ***	Model 2 ***	OxCal Function	Site	Ref ****	Elevation m *****
QL	4650	C20 (1)	D	Fl	charcoal	450	70	Include	Include	Phase	SMF North Shoreline	G96	13
Dry period before Lake C or Maximum age of Lake C													
CAMS-LLNL	75451	SB 3DIII-40 /wd	D	Ae or De	wood	380	50	Include	Include	Phase	CCF South Break	O01	−4
UCIAMS	47204	IFD-T2-C36	342	La	charcoal	380	15	Include	Include	Phase	Imperial Dogwood Rd	R11	−32
AA	11063	C21a	F1	La	charcoal	387	55	Include	Include	Phase	SMF North Shoreline	G96	13
CAMS-LLNL	128362	Sb3m59A-c	3L	La	charcoal	435	35	Include	Include	Phase	SAF Coachella	P11	9
CAMS-LLNL	75462	SB 3DIII-40 /hu	D	Ae or De	humic	460	60	Include	Include	Phase	CCF South Break	O01	−4
UCIAMS	35449	T2-Sb2-3-c	3L	La	charcoal	530	15	Include	Include	Phase	SAF Coachella	P11	9
CAMS-LLNL	125190	Nb2m30A-b-hum	3L	La	humic	545	40	Include	Include	Phase	SAF Coachella	P11	9
UCIAMS	35448	T2-Sb2-2-c	3L	La	charcoal	580	15	Include	Include	Phase	SAF Coachella	P11	9
CAMS-LLNL	125110	Nb2m30A-b-AAA	3L	La	AAA	585	30	Include	Include	Phase	SAF Coachella	P11	9
UCIAMS	47190	IFD-T2-C47	356	La	charcoal	605	15	Include	Include	Phase	Imperial Dogwood Rd	R11	−32
UCIAMS	35629	T2-Sb2-9-c	3L	La	charcoal	605	20	Include	Include	Phase	SAF Coachella	P11	9
UCIAMS	35454	T2-Sb2-17-c	3L	La	charcoal	610	15	Include	Include	Phase	SAF Coachella	P11	9
UCIAMS	47194	IFD-T2-C11	349–354	La	charcoal	610	15	Include	Include	Phase	Imperial Dogwood Rd	R11	−32
CAMS-LLNL	128264	Nb3m41A-b-hum	4Sc	La	humic	610	30	Include	Include	Phase	SAF Coachella	P11	9
CAMS-LLNL	97481	SMF-S28	Q4	La	organic mat	610	40	Include	Include	Phase	SMF South Shoreline	F05	13
AA	9493	C14	G3	Fl	charcoal	615	60	Include	Include	Phase	SMF North Shoreline	G96	13
UCIAMS	48828	IFD-T5-C80	348–358	La	charcoal	615	15	Include	Include	Phase	Imperial Dogwood Rd	R11	−32
UCIAMS	48829	IFD-T5-C84	348–358	La	charcoal	625	15	Include	Include	Phase	Imperial Dogwood Rd	R11	−32
UCIAMS	47189	IFD-T2-C45	354/356	La	charcoal	625	15	Include	Include	Phase	Imperial Dogwood Rd	R11	−32
UCIAMS	47192	IFD-T2-C20	342/344	La	charcoal	630	15	Include	Include	Phase	Imperial Dogwood Rd	R11	−32
UCIAMS	48827	IFD-T5-C79	348–358	La	charcoal	630	15	Include	Include	Phase	Imperial Dogwood Rd	R11	−32
UCIAMS	47191	IFD-T2-C21	336	La	charcoal	640	15	Include	Include	Phase	Imperial Dogwood Rd	R11	−32
UCIAMS	88837	IFD-T9-C320	358/361	La	charcoal	640	30	Include	Include	Phase	Imperial Dogwood Rd	R11	−32
AA	11062	C20 (2)	F1	La	charcoal	643	60	Include	Include	Phase	SMF North Shoreline	G96	13
CAMS-LLNL	128352	Nb3m41A-b-AAA	4Sc	La	AAA	645	30	Include	Include	Phase	SAF Coachella	P11	9
UCIAMS	47187	IFD-T2-C44	342/344	La	charcoal	655	15	Include	Include	Phase	Imperial Dogwood Rd	R11	−32
UCIAMS	47188	IFD-T2-C49	346	La	charcoal	655	15	Include	Include	Phase	Imperial Dogwood Rd	R11	−32
UCIAMS	88833	IFD-T3-C180	360–385 (?)	La	charcoal	660	25	Include	Include	Phase	Imperial Dogwood Rd	R11	−32
CAMS-LLNL	128265	Nb2m44A-b-AAA	3L	La	AAA	665	30	Include	Include	Phase	SAF Coachella	P11	9
CAMS-LLNL	128353	Nb2m44A-b-hum	3L	La	humic	700	30	Include	Include	Phase	SAF Coachella	P11	9
AA	9492	C9	G3	Fl	charcoal	700	55	Include	Include	Phase	SMF North Shoreline	G96	13
CAMS-LLNL	125111	Nb3m20A-b-AAA	4Se	La	AAA	700	30	Include	Include	Phase	SAF Coachella	P11	9
CAMS-LLNL	125191	Nb3m20A-b-hum	4Se	La	humic	705	35	Include	Include	Phase	SAF Coachella	P11	9
CAMS-LLNL	128356	Nb4m28B-c	4Sf	Fl	charcoal	815	35	Include	Include	Phase	SAF Coachella	P11	9
AA	9490	C21b	F1	La	charcoal	905	60	Include	Include	Phase	SMF North Shoreline	G96	13
UCIAMS	35422	Sb3m4B-b-hum	4Sg	Fl	humic	915	15	Include	Not Dry?	Phase	SAF Coachella	P11	9
UCIAMS	35450	T2-Sb2-4-c	4S	Fl or La	charcoal	930	15	Include	Not Dry?	Phase	SAF Coachella	P11	9

Table 1 (*continued*)

Lab Code *	Lab Sample #	Sample Name	Stratigraphic Unit	Depositional Environment **	Material	^{14}C age yr	± yr	Model 1 ***	Model 2 ***	OxCal Function	Site	Ref ****	Elevation m *****
Dry period before Lake D or Maximum age of Lake D													
UCIAMS	35444	Sb4m26A-c	4La	La	charcoal	890	15	Poor Fit	Include	Phase	SAF Coachella	P11	9
UCIAMS	35628	Sb3m49A-b-hum	5S	De or La	humic	910	20	Include	Include	Phase	SAF Coachella	P11	9
UCIAMS	35429	Sb3m49A-b-AAA	5S	De or La	AAA	915	20	Include	Include	Phase	SAF Coachella	P11	9
CAMS-LLNL	128261	Nb5m28B-b-AAA	5S	De or La	AAA	935	30	Include	Include	Phase	SAF Coachella	P11	9
UCIAMS	35451	T2-Sb2-6-c	4L	La	charcoal	945	15	Include	Include	Phase	SAF Coachella	P11	9
CAMS-LLNL	128262	Nb5m28B-b-hum	5S	De or La	humic	955	30	Include	Include	Phase	SAF Coachella	P11	9
UCIAMS	35446	Sb4m27B-c	4La	La	charcoal	960	15	Include	Include	Phase	SAF Coachella	P11	9
CAMS-LLNL	128256	T2-Sb2-1-b-AAA	5Sa	De or La	AAA	960	30	Include	Include	Phase	SAF Coachella	P11	9
CAMS-LLNL	125218	Sb4m49B-b-hum	5S	De or La	humic	965	30	Include	Include	Phase	SAF Coachella	P11	9
UCIAMS	35445	Sb4m27A-c	4La	La	charcoal	980	15	Include	Include	Phase	SAF Coachella	P11	9
CAMS-LLNL	73111	3012	161	La	charcoal	980	30	Include	Include	Phase	SMF Carrizo Wash	R03	8
CAMS-LLNL	128351	Nb3m65B-b-AAA	5S	De or La	AAA	985	30	Include	Include	Phase	SAF Coachella	P11	9
CAMS-LLNL	128263	Nb3m65B-b-hum	5S	De or La	humic	995	35	Include	Include	Phase	SAF Coachella	P11	9
CAMS-LLNL	125217	Sb4m49B-b-AAA	5S	De or La	AAA	1030	35	Poor Fit	Include	Phase	SAF Coachella	P11	9
Dry period before Lake E or Maximum age of Lake E													
UCIAMS	90991	IFD-T4-C412	420 ddd–f	La	charcoal	845	15	Poor Fit	Not Dry?	Phase	Imperial Dogwood Rd	R11	−32
CAMS-LLNL	128361	Sb3m7A-c	5Ld	La	charcoal	955	30	Include	Not Dry?	Phase	SAF Coachella	P11	9
UCIAMS	75459	IFD-T2-C140	390	Bl	charcoal	1010	20	Include	Include	Phase	Imperial Dogwood Rd	R11	−32
UCIAMS	35424	Sb3m11A-c	5Ld	La	charcoal	1075	15	Include	Include	Phase	SAF Coachella	P11	9
UCIAMS	35420	Sb3m3B-c	5Ld	La	charcoal	1095	20	Include	Include	Phase	SAF Coachella	P11	9
CAMS-LLNL	128040	T9-103	160	La	charcoal	1100	30	Include	Include	Phase	SMF Carrizo Wash	This	8
UCIAMS	35419	Sb3m3A-c	5Ld	La	charcoal	1150	15	Include	Include	Phase	SAF Coachella	P11	9
Dry period before Lake F or Maximum age of Lake F													
UCIAMS	35416	Sb3m0B-c	6La SW	La	charcoal	1080	15	Include	Include	Phase	SAF Coachella	P11	9
UCIAMS	35417	Sb3m1B-c	6La SW	La	charcoal	1105	15	Include	Include	Phase	SAF Coachella	P11	9
UCIAMS	35407	Nb4m13B-c	6La SW	La	charcoal	1125	20	Include	Include	Phase	SAF Coachella	P11	9
CAMS-LLNL	73106	3001b	156	La	charcoal	1160	40	Include	Include	Phase	SMF Carrizo Wash	R03	8
CAMS-LLNL	128355	Nb4m13A-c	6Lb SW	La	charcoal	1185	30	Include	Include	Phase	SAF Coachella	P11	9
CAMS-LLNL	128359	Sb4m14A-c	7S SW	Fl	charcoal	1185	30	Include	Include	Phase	SAF Coachella	P11	9
		662001-1	157b	De or La	charcoal	1710	50	Include	Include	Phase	SMF Carrizo Wash	R03	8
UCIAMS	90988	IFD-T4-C406b	550–560 (?)	De or La or Bl	charcoal	1965	15	Include	Include	Phase	Imperial Dogwood Rd	R11	−32
UCIAMS	90985	IFD-T4-C398	501/510	La	charcoal	2035	15	Include	Include	Phase	Imperial Dogwood Rd	R11	−32
UCIAMS	90987	IFD-T4-C404	550–560 (?)	De or La or Bl	charcoal	2100	90	Include	Include	Phase	Imperial Dogwood Rd	R11	−32
UCIAMS	75461	IFD-T3-C159	501/510 FF	La (FF)	charcoal	2230	20	Include	Not Dry?	Phase	Imperial Dogwood Rd	R11	−32
UCIAMS	88835	IFD-T3-C200	500–501	La	charcoal	2275	25	Include	Not Dry?	Phase	Imperial Dogwood Rd	R11	−32
UCIAMS	90989	IFD-T4-C407	550–560 (?)	De or La or Bl	charcoal	2280	15	Poor Fit	Not Dry?	Phase	Imperial Dogwood Rd	R11	−32
UCIAMS	90557	IFD-T4-C362	503	Bl	charcoal	2330	15	Poor Fit	Not Dry?	Phase	Imperial Dogwood Rd	R11	−32
UCIAMS	75462	IFD-T1-C163	580	La	charcoal	2345	20	Poor Fit	Not Dry?	Phase	Imperial Dogwood Rd	R11	−32
UCIAMS	88836	IFD-T3-C204	480	Bl	charcoal	2355	35	Poor Fit	Not Dry?	Phase	Imperial Dogwood Rd	R11	−32
Dry period before Lake G or Maximum age of Lake G													
UCIAMS	90984	IFD-T4-C394b	600	La	charcoal	2115	15	Poor Fit	Include	Phase	Imperial Dogwood Rd	R11	−32

(*continued on next page*)

Table 1 (*continued*)

Lab Code *	Lab Sample #	Sample Name	Stratigraphic Unit	Depositional Environment **	Material	^{14}C age yr	± yr	Model 1 ***	Model 2 ***	OxCal Function	Site	Ref ****	Elevation m *****
UCIAMS	90983	IFD-T4-C390	600	La	charcoal	2190	110	Include	Include	Phase	Imperial Dogwood Rd	R11	−32
UCIAMS	90986	IFD-T4-C402	600	La	charcoal	2550	45	Include	Include	Phase	Imperial Dogwood Rd	R11	−32

* **Lab codes:** AA: NSF—Arizona AMS Facility at University of Arizona, Beta: Beta Analytic, CAMS-LLNL: Center for AMS at Lawrence Livermore National Lab, La Jolla: Scripps (now University of California San Diego), QL: Quaternary Isotope Lab (now University of Washington), TO: University of Toronto, UCIAMS: Keck—Carbon Cycle AMS Facility at University of California Irvine, UCLA: University of California Los Angeles, UCR: University of California Riverside, UGa: University of Georgia, Umich: University of Michigan.
** **Depositional environment abbreviations:** Ae: Aeolian, Bl: Sand blow, Bu: Burn horizon, Cu: Cultural, De: Deltaic, Fl: Fluvial, La: Lacustrine, Sh: Shoreline berm.
*** **Explanation of terms for Model 1 & 2 columns:** "Include": Date included in model. "Poor Fit": Date excluded a posteriori because the agreement index in OxCal was below 60%. "Not Dry?": Date excluded a priori in Model 2 as possibly coinciding with a lake highstand, as it does not cluster with other dates in the same lake package.
**** **References:** F05: Faneros (2005), G96: Gurrola and Rockwell (1996), H12: Haaker (2012), J15: Jerrett (2015), L97a: Arkush (1990) in Laylander (1997), L97b: Schaefer (1987) in Laylander (1997), L97c: Schaefer and Pallette (1993) in Laylander (1997), L97d: Yohe (1990) in Laylander (1997), M06: Meltzner et al. (2006), O01: Orgil (2001), P11: Philibosian et al. (2011), P95: Pollard and Rockwell (1995), R03: Ragona (2003), R11: Rockwell et al. (2011), S90: Sieh and Williams (1990), This: This paper, W15: Wessel (2015), W17: White (2017).
***** **All elevations given relative to present mean sea level.**

quite distinctive from the clay strata that are interpreted to represent deeper water deposition. Where overlain by clayey lake strata, the deltaic deposits are interpreted to be essentially the same age as the overlying lacustrine deposits as they likely represent the filling phase of the same lake.

Sediments interpreted as fluvial in origin, "Fl" in Table 1, are present between lake deposits at some localities (Gurrola and Rockwell, 1996; Faneros, 2005; Meltzner et al., 2006; Philibosian et al., 2011; Rockwell et al., 2011; Jerrett, 2015), and these demonstrably indicate a separation of one lake from another in that they must represent a "dry period" between lakes, or at least some lowering of the lake during a dry period. Samples from these deposits date a dry period prior to the overlying lake, but because of inheritance of older, sometimes reworked charcoal, they can be substantially older than the overlying lake strata.

Possible aeolian deposits, indicated "Ae", are found at a few sites (Orgil, 2001; Ragona, 2003; Philibosian et al., 2011), and they would indicate subaerial deposition, and therefore a lack of lake water. Samples recovered from these deposits give a maximum age for the overlying lake strata.

A few dates are on samples recovered from in situ surface burns at elevations below the highstand shoreline of Lake Cahuilla (Meltzner et al., 2006) and are indicated "Bu" in Table 1. These surfaces must represent a period of no water at the site.

Samples recovered from shoreline berm deposits ("Sh" in Table 1; e.g., Gurrola and Rockwell, 1996; Faneros, 2005; Philibosian et al., 2011; White, 2017) may be as young as the lake itself, although detrital charcoal still provides maximum ages (terminus post quem) for a lake. Eight of the dates in our model from shoreline berms are cultural and associated with an archeological site ("Cu" in Table 1). Some of these lend confirmation towards a post-1700 date for the most recent filling of Lake Cahuilla.

A number of the dated samples in our compilation originate from organic mats. The organic mats range from millimeters to a centimeter in thickness, and they were found exclusively at sites at an elevation between +9 m and +13 m, at or within 0.5 km of the highstand shoreline. These organic layers typically have sharp upper and lower contacts and are commonly interbedded with beach berm deposits. They are interpreted as the organic detritus that floated or was washed to the shoreline during inundation (Gurrola and Rockwell, 1996). Organic mats such as these rarely survive prolonged exposure, so their preservation in the sedimentary record is most readily explained if they were quickly buried by deltaic or littoral deposits in one or more storms in the same year. Fig. 2 compares an organic mat at the Gurrola and Rockwell (1996) site with the organic detritus that accumulated along the shore of nearby Laguna Salada during its filling in 1984, which we interpret as an analogous event: the material is strikingly similar in composition, and the organic detritus at Laguna Salada was subsequently buried by berm deposits produced by wind-driven waves.

3.2. Radiocarbon constraints: dated materials

Several types of organic materials have been collected and dated at the various sites around the basin. The most common are detrital charcoal; organic mat deposits or components therein (including humic acid dates); wood (including one humic acid date on a sample of wood); dead stumps in growth position buried by lake deposits; fish bone; and shell.

Many aspects of radiocarbon dating must be considered carefully in order to precisely and accurately determine the chronology of Lake Cahuilla. For charcoal, the "old wood problem" is well-recognized in archeological and paleoseismological studies (Blong and Gillespie, 1978; Schiffer, 1986; Erlandson and Rockwell, 1987; Gavin, 2001), as radiocarbon dates determine the time of wood growth and death, which for most vascular plants is the same year. As there must be some time lag between annual wood growth, the burning of the wood, and its transport and deposition, all radiocarbon dates on detrital charcoal have some age inheritance relative to the sediments that contain them. In the arid Salton Trough, this inheritance problem may be particularly noteworthy: the valley bottom below the shoreline of Lake Cahuilla is unlikely to burn in wildfires, as the vegetation density is low (Anderson et al., 2022; Monitoring Trends in Burn Severity MTBS, 2022). In contrast, there is abundant dry wood scattered across the basin floor, including above the shoreline, that may have been dead for a long time. The Cahuilla and Kumeyaay tribes needed wood for cooking fires (Aschmann, 1959; Weide, 1974; Wilke, 1978; Laylander, 1997), and the dry wood on the basin floor could have been easily utilized for this purpose; this may be the most common source of charcoal in our study area.

Many of the charcoal samples collected from sites at or below the highstand shoreline were observed as distributed or rare pieces within lacustrine and deltaic strata. The wood that burned to produce the charcoal would not have grown underwater, except for some woody vegetation that may have grown at the shoreline, and this raises an additional question: was the charcoal introduced from outside the lake footprint, or did it grow on the desert floor during dry periods and then get incorporated into the lake deposits during the inundation and lake phases? At the Imperial fault site at Dogwood Road, 16 km from the highstand shoreline, some charcoal

Fig. 2. The organic mat layers at the Northern Shoreline Site (upper right; Gurrola and Rockwell, 1996) are composed of charcoal and carbonized twigs, leaves, grass blades, and seeds. They are strikingly similar in composition to the organic detritus resulting from the 1984 flooding of Laguna Salada; the left photo shows an accumulation of organic detritus at the Laguna Salada shoreline that was subsequently buried by berm deposits produced by wind-driven waves. Based on the similarity between the deposits, we infer the organic mat deposits in Lake Cahuilla were also formed during inundation events. In the vertical trench exposure (upper right), the yellow-and-blue flagged nails define a stratigraphic contact; the dark organic mat below the nails is ~1 cm thick, and the field of view is roughly 20–25 cm wide. (For interpretation of the references to colour in this figure legend, the reader is referred to the Web version of this article.)

was found in clusters with as many as 30–50 pieces in a single bedded lacustrine stratum within a small, <1 m area (Rockwell et al., 2011). Such a dense cluster of charcoal is unlikely to have accumulated in a non-channelized deposit if the individual pieces had each floated in from beyond the distant shoreline; the wood is more likely to have grown and been burned nearby during a preceding dry period.

The organic mats are composed of organic detritus, including detrital charcoal, carbonized or charred twigs, carbonized seeds, wood, and carbonized leaves and grass fragments. Accelerator mass spectrometry (AMS) dating of different components extracted from individual organic mats has yielded suites of ages, each of which generally clusters about a common age, but which may have some components that are significantly older. The cluster of ages implies that most of the material likely grew within the lake footprint during the dry interval immediately prior to inundation, though a small fraction of the material may have grown during an earlier dry period or may have come in from beyond the lake shoreline when the lake was full.

Some of the dates on the organic layers are bulk dates where the entire stratum was dated. These fall into two categories: material with pretreatment limited to acid-only washing (described in Table 1 as "organic mats") versus bulk dates, also on organic mats, where the sample was washed in acid, alkali, and then more acid (referred to as "AAA" in Table 1). In our model, we treat the organic mat and AAA dates similarly. Because organic bulk dates contain a suite of materials that may span the preceding dry period, they represent not only a maximum age (terminus post quem) for the overlying lake deposits, but multiple organic bulk dates from the same horizon may help map out the extent of the preceding dry period. However, as there is little data on the preservation potential for organic material from early in a long dry period, the organic bulk dates may not map out the entirety of the preceding dry period. Additionally, as the organic bulk dates may contain still older charcoal, care must be taken to avoid overinterpreting individual, particularly isolated dates. Consequently, all of these organic bulk dates are expected to be older than the overlying lake stratum itself, but many dates will have only the inheritance that is residual from some portion of the immediately preceding dry phase.

Some dates were run on wood. Most of these are from the in situ mesquite stumps dated by Rockwell et al. (2018). These stumps were surrounded by coppice dunes that were covered in gastropod shells (*Physa humerosa*) from at least one lake inundation. The trees necessarily grew during some dry period prior to the most recent Lake Cahuilla highstand, and based on the ages of these stumps (some date to ~1700 CE or later) it is clear they are too young to have grown prior to the penultimate lake, so they must date the dry interval immediately prior to the most recent highstand.

In each case, the stump was sawed from its base and collected in its entirety, and the innermost and outermost 2–3 rings were sampled separately for radiocarbon dating (Rockwell et al., 2018). The respective dates from the inner and outer samples from each stump were paired together and nested in a sequence in the age model; growth rings were assumed to be annual, and the number of rings between the paired inner and outer samples was estimated and included in the age model as an additional constraint.

Composite charcoal dates (samples with multiple fragments of charcoal that are derived from different-aged pieces) are not used in the OxCal models that we present below, because an average of two detrital charcoal ages from different dry periods may not itself date a dry period. Additionally, we do not include fish bone and shell in our analysis because of the poorly constrained and potentially different radiocarbon reservoir corrections (R) that would be required to compare the various samples in the same model.

3.3. Summary of stratigraphic sites used in this study

Radiocarbon data from paleoseismic sites with constraints on lake stratigraphy (Sieh and Williams, 1990; Pollard and Rockwell, 1995; Gurrola and Rockwell, 1996; Thomas and Rockwell, 1996; Orgil, 2001; Ragona, 2003; Verdugo, 2004; Faneros, 2005; Meltzner et al., 2006; Philibosian et al., 2011; Rockwell et al., 2011; Jerrett, 2015; Wessel, 2015), a shoreline site (White, 2017), several archeological sites (Laylander, 1997), and scattered mesquite stumps (Haaker, 2012; Rockwell et al., 2018) have been compiled and considered in this analysis (Supplementary Table S1). Only some of the sites are previously published, but all unpublished dates are contained in MS theses at San Diego State University (SDSU) or in accessible technical reports, and a summary of the stratigraphic context of each date is provided in Supplementary Text S1 and Supplementary Figs. S1–S20. A brief overview of each site is provided here for context; see the supplementary material for a more complete description as well as a stratigraphic column for each site.

3.3.1 San Andreas fault sites

Three paleoseismic sites have been developed along the southernmost section of the San Andreas fault at or below the highstand shoreline of Lake Cahuilla: the Indio, Coachella, and Salt Creek sites. The Indio (Sieh, 1986) and Salt Creek (Williams, 1989) sites were never formally published so the radiocarbon dates published in abstract form are of limited use. However, some data are presented by Sieh and Williams (1990). The Coachella site (Philibosian et al., 2011) has a rich record of lakes and dates and provides the best chronologic and stratigraphic data from the northeastern margin of Lake Cahuilla.

3.3.2 Imperial and Brawley fault sites

Four sites have been studied along the Imperial and Brawley faults that yielded useful age data: the Brawley site at Harris Road (Meltzner et al., 2006), the Imperial site at Dogwood Road (Rockwell et al., 2011), and the northern (Jerrett, 2015; Wessel, 2015) and southern Imperial Border sites (Thomas and Rockwell, 1996).

3.3.3 San Jacinto fault sites

Five paleoseismic sites have been developed along strands of the southern San Jacinto fault that provide useful stratigraphic and age information for Lake Cahuilla: the Superstition Mountain Fault (SMF) South Shoreline (Faneros, 2005); SMF North Shoreline (Gurrola and Rockwell, 1996); Carrizo Wash (Ragona, 2003; Verdugo, 2004); Coyote Creek Fault (CCF) South Break (Orgil, 2001); and CCF Middle Break Northern Shoreline (Pollard and Rockwell, 1995) sites.

3.3.4 Other sites

Limited radiocarbon data are summarized from other sites, including the Carrizo South Shoreline site (White, 2017), which lies ~2 km east of the Gurrola and Rockwell (1996) site, and from a study of dead stumps that were inundated by the last Cahuilla highstand (Haaker, 2012; Rockwell et al., 2018).

3.3.5 Archeological sites

A number of data are also compiled from archeological sources that document periods of occupation at the shoreline during a lake highstand (Schaefer, 1987; Arkush, 1990; Yohe, 1990; Schaefer and Pallette, 1993; Laylander, 1997).

3.4. The base OxCal model (Model 1)

Of the 423 radiocarbon dates compiled for this assessment, 127 samples (black samples in Supplementary Table S1) were excluded a priori either because (1) a sample yielded a modern date, was assessed by the original authors to be a root, was collected from artificial fill, or had uncertain stratigraphic context; (2) a date was not ^{13}C corrected; or (3) there was an irregularity in date reporting. We also removed 12 samples (gray samples in Supplementary Table S1) that were collected from below a local unconformity where the specific lake associated with the sample could not be independently correlated. The remaining 284 samples have good stratigraphic control.

Next, we removed 120 samples (red samples in Supplementary Table S1) where the calibrated dates were older than the calibrated dates of two or more samples from underlying lakes (with fewer than 20 years of overlap between the respective 2σ probability density functions). Here we imposed a requirement that at least two samples from underlying lakes must be younger in order to remove a sample, to avoid potentially biasing the model by a single young outlier in an underlying lake. The 120 samples that were removed at this stage are interpreted as having age inheritance and therefore not representing the dry period immediately preceding the lake package they were found in. Notably, more than 40% of all stratigraphically well-defined dates (120 of 284) are out of sequence and clearly older than a stratigraphically lower lake, demonstrating significant age inheritance beyond the calibrated age uncertainty.

The reduced set of dates contains 164 stratigraphically consistent radiocarbon dates from sites within the Lake Cahuilla footprint or at the +13 m highstand shoreline (Supplementary Table S1). Of these dates, 10 were found at the +13 m shoreline and have cultural context: nine from archeological sites (Laylander, 1997) and one from a paleoseismic site (Pollard and Rockwell, 1995). All 10 dates provide information on the timing of an Indigenous American occupation and therefore a maximum age (terminus post quem) for the most recent lake highstand. An additional 154 samples were collected for geological studies and comprise detrital charcoal; wood; organic matter in condensed organic mats that include seeds, charcoal, charred twigs, wood, and leaves, most of which likely grew within the lake footprint during dry conditions and were drowned by the lake infilling; in situ stumps that also grew during dry conditions and were presumably drowned by the lake infilling; and humic acid dates on wood samples or other organic matter. These geological sites have the advantage of placing dates into a stratigraphic context where the samples can be related to a particular lake or inter-lake period.

We attempted to run an OxCal model with these 164 dates, grouping the samples in Phases according to the specific dry period they are inferred to have grown in, with the cultural samples from the shoreline providing only a maximum age constraint on the most recent highstand shoreline. However, a problem arose with one sample (Sb3m2A-c) that has a mean calibrated age ~600 years younger than any other sample at the same stratigraphic position and ~700 years younger than multiple samples that were stratigraphically higher: this sample caused the OxCal model to fail, i.e., OxCal yielded a “NULL distribution” error. After removing sample Sb3m2A-c, which we speculate was a root and treat as an outlier, we reattempted the OxCal model. This time, the model ran successfully (“Model 1: Initial Run” in Supplementary Text S2), but 12 dates yielded poor agreement indices (roughly equivalent to χ^2 test failure at 5%; Bronk Ramsey, 1995, 2009b). In our base model (Model 1) we assume the dates with poor agreement indices represent additional outliers. We thus removed the inferred outliers and reran the model with the remaining 151 dates, resulting in

a final base model ("Model 1: Final Version" in Supplementary Text S2; "Model 1" in Supplementary Table S1; Supplementary Fig. S21). In an alternative model (Model 2), discussed next, we will revisit the assumption that the dates with poor agreement indices are necessarily all outliers.

3.5. An alternative OxCal model (Model 2)

As discussed above, we assumed that each date with a poor agreement index in the initial run of Model 1 is an outlier and therefore does not represent the dry period immediately preceding the lake package the sample was found in. However, if OxCal encounters a conflict between dates in two sequential Phases (in two different lake packages) and the two Phases are not sampled evenly, the sampling bias may lead OxCal to prefer the dates in the more densely sampled lake, at the expense of the more sparsely sampled lake. In particular, the seventh lake back (Lake G) was exposed at only a few sites, in most cases below an unconformity, and only three useful dates that are definitively from this lake episode have so far been obtained at any site in the basin (Supplementary Table S1). In Model 1, our rule of using at least two dates from Lake G to determine which dates in Lake F are "too old" results in the inclusion of six dates in Lake F that are older than the youngest date in Lake G. OxCal flags the oldest four dates from Lake F and, importantly, also the youngest date from Lake G for having poor agreement (Supplementary Fig. S21), and those five dates are thus excluded from the final version of Model 1.

In order to test the sensitivity of the OxCal model to the sparse sampling from Lake G, we consider an alternative OxCal model (Model 2) in which all three Lake G dates are assumed to be robust, and we remove the six oldest dates from Lake F a priori (orange samples in Supplementary Table S1; purple dates on Supplementary Fig. S22).

At this stage, we also consider that there may be isolated samples that came in from above the lake shoreline and do not necessarily date a dry period between lakes. We bear in mind that samples that grew within the footprint of Lake Cahuilla would have ages that cluster during the various dry periods between lakes, but samples that grew above the Lake Cahuilla highstand shoreline should have ages that are randomly distributed with respect to the precise Lake Cahuilla chronology. To identify samples that are (slightly) more likely to date a period when the lake was full, we searched for isolated dates at either the young end or the old end of a dry period that do not cluster with other dates from within that package. Aside from sample Sb3m2A-c, which would not run in the OxCal model regardless, we identify two such cases: two dates at the old end of the dry period before Lake C and two dates at the young end of the dry period before Lake E.

In total, in Model 2 we removed 10 dates a priori from the 164 stratigraphically consistent radiocarbon dates discussed in the previous section (orange samples in Supplementary Table S1; purple dates on Supplementary Fig. S22), and additionally we again exclude sample Sb3m2A-c. We ran the OxCal model with the remaining dates ("Model 2: Initial Run" in Supplementary Text S2), but four dates still yielded poor agreement indices. We then removed these four dates and reran the model with the remaining 149 dates, resulting in a final alternative model ("Model 2: Final Version" in Supplementary Text S2; "Model 2" in Supplementary Table S1; Supplementary Fig. S22).

4. Results

4.1. The base OxCal model (Model 1)

Fig. 3 and Supplementary Fig. S21 show an OxCal plot of 295 of the 296 radiocarbon dates for which there is some stratigraphic control, including those samples collected from below a stratigraphic unconformity, but they do not plot the 127 black dates in Supplementary Table S1 (excluded for reasons mentioned earlier) nor the one pre-Holocene date (~40 ka). The near-vertical light brown band encompasses the dates used in the base model, with the individual date probability density functions (PDFs) shown in green, yellow, red and gray. PDFs of dates shown in red represent the dates that violate the stratigraphic ordering, being older than dates from underlying lakes; none of the red dates are used in the base model. The gray dates were collected from below local unconformities and do not necessarily provide age information for the dry period immediately preceding a lake; none of the gray dates are used in the base model. The dates in yellow represent one date that would not run in OxCal and additional dates with poor agreement indices that were excluded from the final base model; we omitted the yellow dates as outliers. Only those dates in green were included in the final model.

Supplementary Figs. S23 and S24 show the "multiple" plots from OxCal for the initial and final runs of Model 1, before and after removing outliers, respectively. Fig. 4a summarizes these results, showing the PDFs for the lake ages from the final run of Model 1. Note that for Lake A, the timing of the beginning and end of the lake highstand are estimated separately, but because the timing of the beginning and end are indistinguishable, we simply combine them as the timing of the highstand itself. The modeled OxCal ages for the lake highstands are 1720–1738 CE (Lake A), 1587–1636 CE (Lake B), 1459–1503 CE (Lake C), 1116–1165 CE (Lake D), 1009–1070 CE (Lake E), 907–966 CE (Lake F), and 612–241 BCE (Lake G). It is important to note that these ages represent the maximum allowable ranges when a lake may have filled the basin up to the highstand elevation: water was not necessarily in the basin for the entirety of each range. Additionally, using the desiccation rate range of 1.52–2.05 m/yr and the filling model of Rockwell et al. (2018), the Colorado River avulsion that initiated the filling may have occurred up to 13–20 years earlier and desiccation may have continued up to 47–64 years later than the respective highstand ranges (green trapezoids, Fig. 4c).

4.2. The alternative OxCal model (Model 2)

Similarly to Supplementary Fig. S21 for Model 1, Supplementary Fig. S22 shows an OxCal plot of the 295 radiocarbon dates for Model 2. The main difference in Model 2 is that 10 PDFs appear in purple, indicating that they were excluded a priori in Model 2, either to test the sensitivity of the OxCal model to the sparse sampling from Lake G or to test its sensitivity to isolated samples that may have come in from above the lake shoreline and do not necessarily date a dry period between lakes. A consequence of excluding these 10 samples a priori is that three dates that had been flagged as outliers in Model 1 now have good agreement with the model, and so have switched from yellow in Model 1 to green in Model 2. Fig. 5 highlights the differences between Models 1 and 2.

Supplementary Figs. S25 and S26 show the "multiple" plots from OxCal for the initial and final runs of Model 2, before and after removing outliers, respectively. Fig. 4b summarizes these results, showing the PDFs for the lake ages from the final run of Model 2, in comparison with those from Model 1. The Model 2 lake highstand possible timings are 1720–1735 CE (Lake A), 1587–1636 CE (Lake B), 1459–1503 CE (Lake C), 1151–1241 CE (Lake D), 995–1042 CE (Lake E), 906–966 CE (Lake F), and 166–5 BCE (Lake G). The biggest differences from Model 1 to Model 2 are in the possible timings of Lakes D, E, and G (Fig. 4a and b). Again, using the desiccation rates and filling model of Rockwell et al. (2018), the Colorado River avulsion that initiated the filling may have occurred up to 13–20

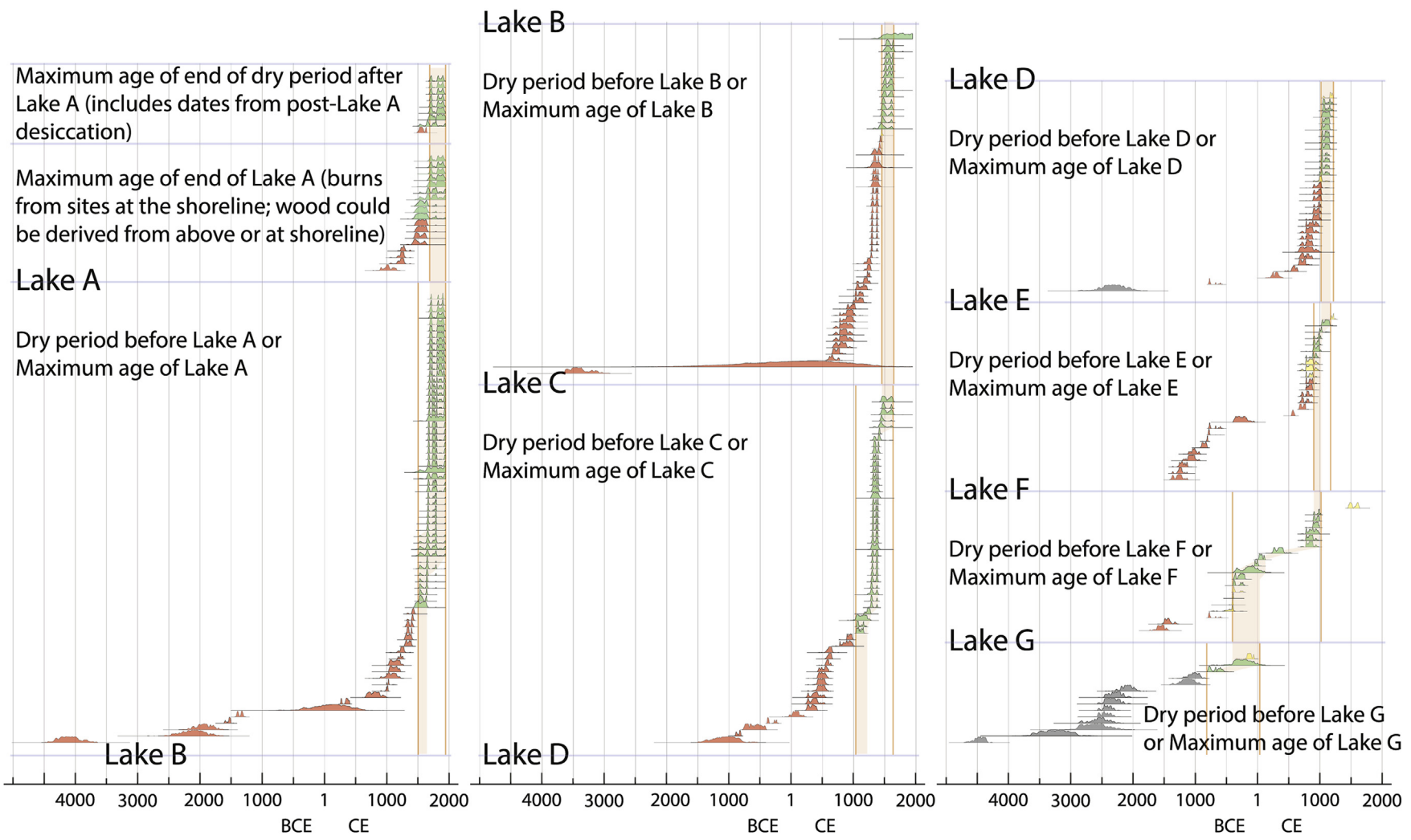

Fig. 3. Plot of all 295 Holocene dates with stratigraphic control, organized by lake and then by relative radiocarbon age; roots and dates from artificial fill are not included. The light brown subvertical bar represents an age bound for consistency: dates that fall to the left of the brown band are considered to have some inherited age; those to the right are likely outliers. The probability density functions (PDFs) shown in green are those that are used in the base model. The PDFs in yellow represent one date that would not run in OxCal and additional dates with poor agreement indices that were excluded from the final base model. The red PDFs are interpreted to have some age inheritance, and the gray PDFs are from samples below a local unconformity. The yellow, red, and gray dates are not used in the base model. See Table 1 and Supplementary Fig. S21 for details. (For interpretation of the references to colour in this figure legend, the reader is referred to the Web version of this article.)

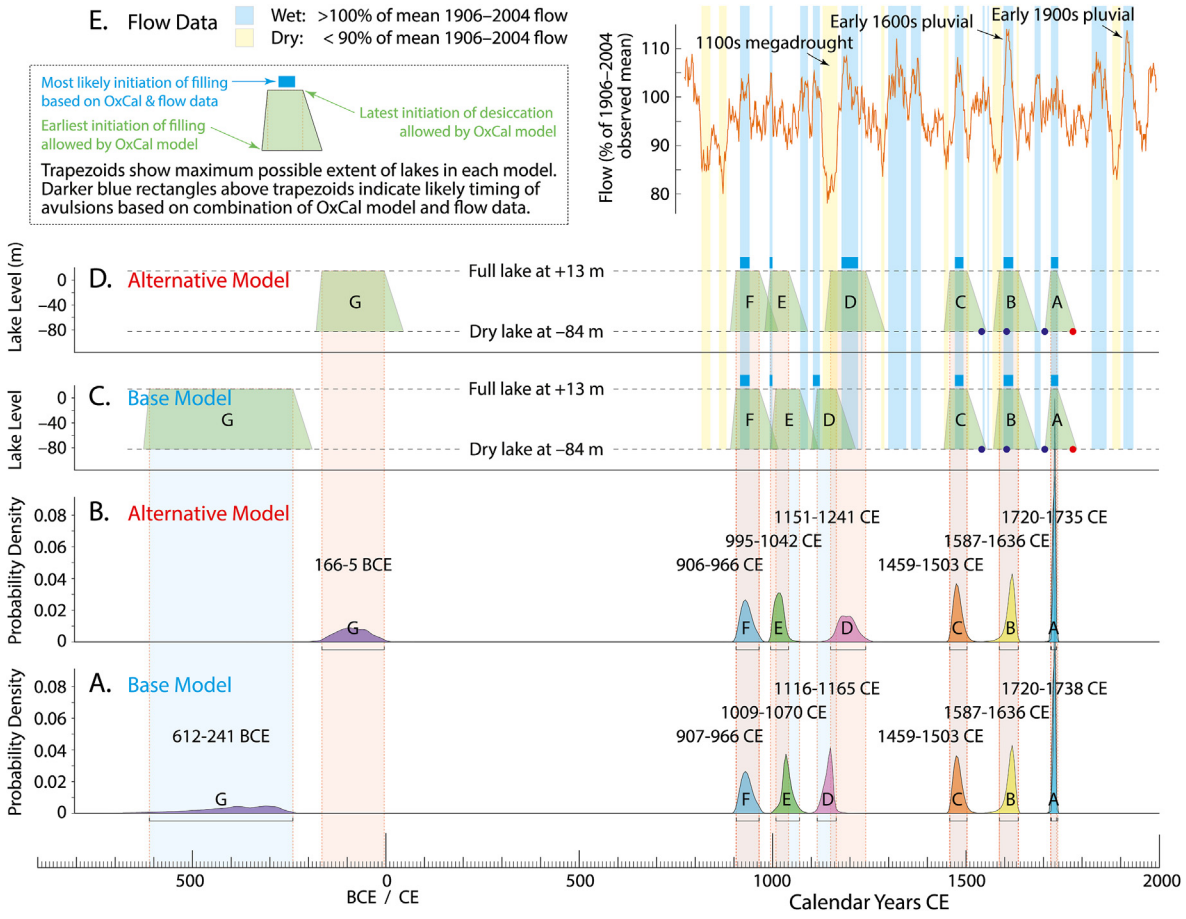

Fig. 4. The base and alternative OxCal models (Models 1 and 2) for Lake Cahuilla highstands compared with a streamflow reconstruction for the upper Colorado River. Probability density functions (PDFs), taken from the OxCal output, are shown for the timing of each lake highstand for the (a) base and (b) alternative models. In each case, these PDFs illustrate the maximum possible extent of the highstand and may overestimate its duration. Differences between the models result from the inclusion or exclusion of specific dates that may or may not be representative of a particular inter-lake dry period. Where the base and alternative models agree, the results are considered robust, but where the models differ, those differences are indicative of real uncertainty in the lake ages. Trapezoids in (c) for the base model and in (d) for the alternative model schematically extend the highstand windows from OxCal (a and b, respectively) to allow 13–20 years for the lake to fill and 47–64 years for it to completely desiccate. The trapezoids are then compared to (e) upper Colorado River flow, shown as a 25-yr moving average and expressed as a % of 1906–2004 mean flow (18.53×10^9 m^3; from Meko et al., 2007, and bias-corrected using quantile mapping by Robeson et al., 2020). The dark blue rectangles immediately above the trapezoids indicate the likely timing of Colorado River avulsions, as determined from the overlap of wet periods in (e) with the portion of each lake between the earliest possible initiation of filling and the end of the highstand, i.e., between the lower left and upper right corners of each trapezoid in (c) and (d). Purple dots in (c) and (d) designate the timing of historical observations that the Colorado River was flowing southward into the Gulf of California (Rockwell et al., 2018); of particular interest is the 1605 observation of Oñate, which would require either that Lake B had already completed filling and had begun desiccating before 1605 or that Lake B began filling only after 1605. The red dot in (c) and (d) marks Anza's visit in 1774, when no water was found in the basin; this requires that Lake A began desiccating no later than 1733 (Rockwell et al., 2018). For Lake A, both the beginning-of-lake and end-of-lake PDFs are retained, but they nearly overlap. Note also that the 1905–1907 flooding of the basin occurred at the onset of the "early 1900s pluvial" of Robeson et al. (2020), which led Ross (2020) to argue that this likely would have completely filled the basin to +13 m had the Colorado River not been redirected back to the Gulf of California by engineers. (For interpretation of the references to colour in this figure legend, the reader is referred to the Web version of this article.)

years earlier and desiccation may have continued up to 47–64 years later than the respective highstand ranges (Fig. 4d).

4.3. Refinement of end of Lake A based on historical accounts

Both the base model and the alternative model suggest a slightly longer window for Lake A compared to the model of Rockwell et al. (2018), 1720–1738 and 1720–1735, respectively, compared to 1719–1733. Rockwell et al. (2018) trimmed their Lake A age on the argument that Lake Cahuilla had mostly or completely desiccated by the time of Anza's visit in 1774, when Anza's party did not report finding water in the Salton Basin. Using plausible desiccation rates, they estimated that the lake must have begun desiccating by the early 1730s in order to be consistent with the historical observations. Following the logic of Rockwell et al. (2018), we also trim the end of the Lake A highstand to 1733 CE.

5. Discussion

5.1. Model comparison and implications of model divergence

The age estimates from the base model and the alternative model generally agree with one another for both Lakes A and B, but as the ages for these two lakes were also estimated previously by Rockwell et al. (2018), it is interesting to compare these new results to those from the earlier study. For Lake A, if historical accounts (Anza's observations in 1774) are considered as noted in the previous section, our new results here agree with those of Rockwell et al. (2018). For Lake B, Rockwell et al. (2018) estimated a comparatively imprecise range of 1509–1644 CE. With the new dates we have added in this paper, we refine the age of the Lake B highstand to sometime in the interval 1587–1636 CE. This new estimate falls entirely within the range estimated by Rockwell et al.

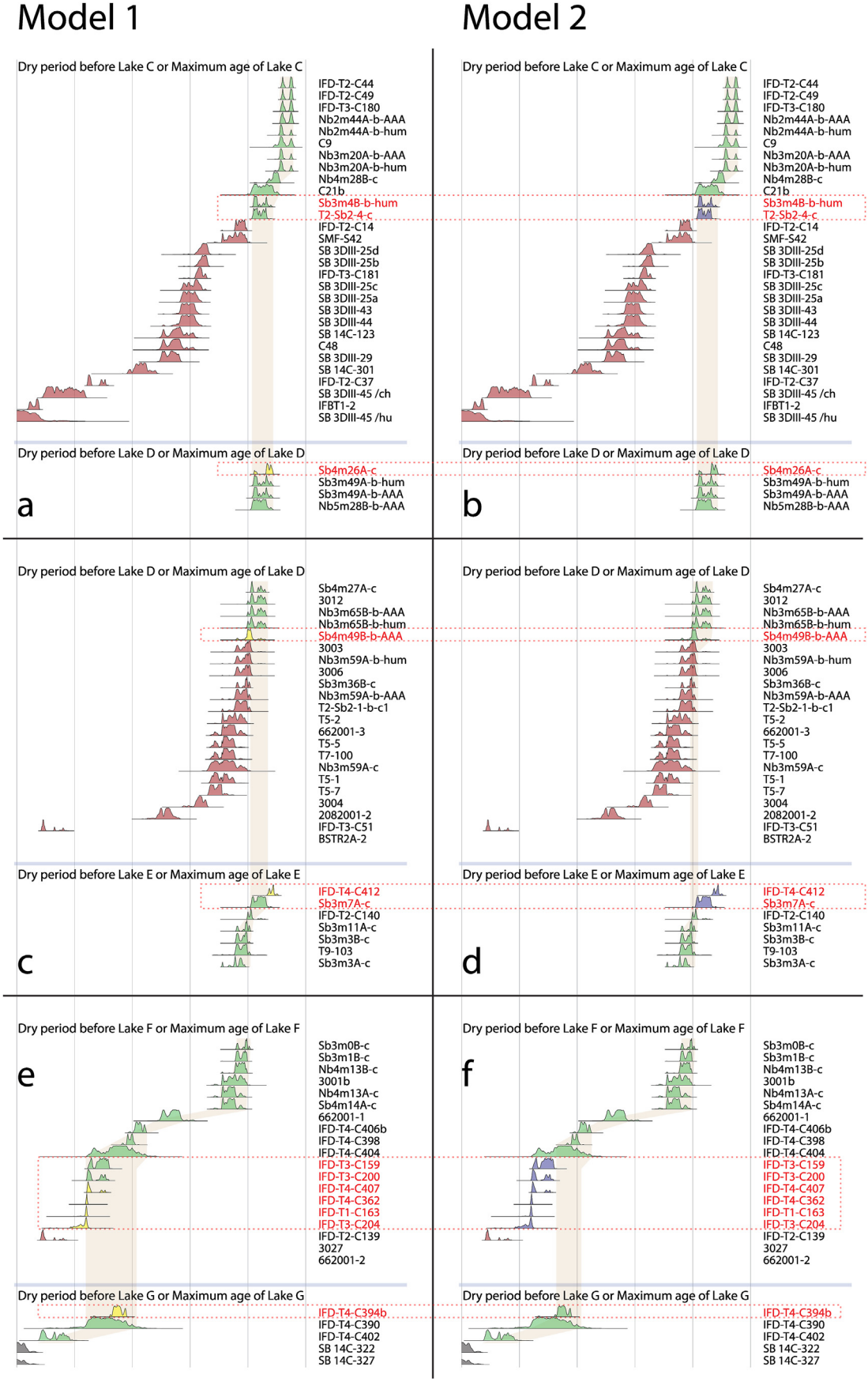
Model 1
Model 2
Dry period before Lake C or Maximum age of Lake C
IFD-T2-C44
IFD-T2-C49
IFD-T3-C180
Nb2m44A-b-AAA
Nb2m44A-b-hum
C9
Nb3m20A-b-AAA
Nb3m20A-b-hum
Nb4m28B-c
C21b
Sb3m4B-b-hum
T2-Sb2-4-c
IFD-T2-C14
SMF-S42
SB 3DIII-25d
SB 3DIII-25b
IFD-T3-C181
SB 3DIII-25c
SB 3DIII-25a
SB 3DIII-43
SB 3DIII-44
SB 14C-123
C48
SB 3DIII-29
SB 14C-301
IFD-T2-C37
SB 3DIII-45 /ch
IFBT1-2
SB 3DIII-45 /hu
Dry period before Lake D or Maximum age of Lake D
Sb4m26A-c
Sb3m49A-b-hum
Sb3m49A-b-AAA
Nb5m28B-b-AAA
a
b
Dry period before Lake D or Maximum age of Lake D
Sb4m27A-c
3012
Nb3m65B-b-AAA
Nb3m65B-b-hum
Sb4m49B-b-AAA
3003
Nb3m59A-b-hum
3006
Sb3m36B-c
Nb3m59A-b-AAA
T2-Sb2-1-b-c1
T5-2
662001-3
T5-5
T7-100
Nb3m59A-c
T5-1
T5-7
3004
2082001-2
IFD-T3-C51
BSTR2A-2
Dry period before Lake E or Maximum age of Lake E
IFD-T4-C412
Sb3m7A-c
IFD-T2-C140
Sb3m11A-c
Sb3m3B-c
T9-103
Sb3m3A-c
c
d
Dry period before Lake F or Maximum age of Lake F
Sb3m0B-c
Sb3m1B-c
Nb4m13B-c
3001b
Nb4m13A-c
Sb4m14A-c
662001-1
IFD-T4-C406b
IFD-T4-C398
IFD-T4-C404
IFD-T3-C159
IFD-T3-C200
IFD-T4-C407
IFD-T4-C362
IFD-T1-C163
IFD-T3-C204
IFD-T2-C139
3027
662001-2
e
f
Dry period before Lake G or Maximum age of Lake G
IFD-T4-C394b
IFD-T4-C390
IFD-T4-C402
SB 14C-322
SB 14C-327

(2018). Nevertheless, the primary reason that the newly-added dates push the onset of Lake B forward by nearly eight decades is because of a double peak at this time in the radiocarbon calibration curve, with the Bayesian trimming algorithm in OxCal now favoring the younger intercept in the calibration curve. In reality, the radiocarbon data cannot strictly distinguish which peak or intercept is correct, so some of the broader age range reported for Lake B by Rockwell et al. (2018) may still be valid.

Going back beyond Lake B, the only significant differences between the base and alternative models are in the possible timings of Lakes D, E, and G. This should not be surprising, considering that those are the lakes most affected by the changes highlighted in Fig. 5. In Model 1 the youngest date in the dry period before Lake D (Sb4m26A-c) was removed a posteriori as an outlier (Fig. 5a), but in Model 2 the a priori removal of the two oldest dates in the dry period before Lake C (Sb3m4B-b-hum and T2-Sb2-4-c) results in the inclusion of Sb4m26A-c, which was not flagged as an outlier in Model 2 (Fig. 5b). The upshot of these changes is a push in the mean age of Lake D forward in time by five decades (Fig. 4a and b and Supplementary Figs. S24 and S26), coupled with an overall broadening of the PDF for Lake D. Similarly, in Model 1 the oldest date in the dry period before Lake D (Sb4m49B-b-AAA) was removed a posteriori as an outlier (Fig. 5c), but in Model 2 the a priori removal of the two youngest dates in the dry period before Lake E (IFD-T4-C412 and Sb3m7A-c) results in the inclusion of Sb4m49B-b-AAA, which was not flagged as an outlier in Model 2 (Fig. 5d). The consequence of these changes is a push in the mean age of Lake E backward in time by two decades (Fig. 4a and b and Supplementary Figs. S24 and S26).

Focusing on Lake G, removing the youngest sample in the preceding dry period has a profound effect on the age of Lake G. In Model 1 the youngest date in the dry period before Lake G (IFD-T4-C394b) was removed a posteriori as an outlier (Fig. 5e), but in Model 2 the a priori removal of the six oldest dates in the dry period before Lake F results in the inclusion of IFD-T4-C394b, which was not flagged as an outlier in Model 2 (Fig. 5f). The result of these changes is a push in the mean age of Lake G forward in time by three centuries (Fig. 4a and b and Supplementary Figs. S24 and S26), coupled with an overall narrowing of the PDF for Lake G.

Reflecting on the differences between the base and alternative models, because we cannot know without additional information whether the assumptions underpinning the alternative model are more defensible than those incorporated into the base model, any differences between the two models should be considered a reflection of the true uncertainty in the lake ages. In particular, the instability in the modeled age for Lake G reveals that additional age constraints on Lake G are still critically needed. For the more recent lakes, in the next section we will explore whether high-resolution paleohydrologic reconstructions can provide additional insight into the likely timing of each lake filling.

5.2. Comparison to streamflow reconstruction and a preferred Lake Cahuilla model

A common hypothesis is that the filling phases of Lake Cahuilla initiate during wet periods in the Colorado River basin and Colorado Plateau, as an avulsion of the Colorado River would be more likely during a period of high discharge (Waters, 1983; Slingerland and Smith, 2004). In an attempt to test this hypothesis, we compare the lake chronology with rainfall estimates based on tree-ring data from the upper Colorado River drainage basin (Meko et al., 2007; Robeson et al., 2020). The Robeson et al. (2020) study applied quantile mapping to correct biases in the historical rainfall and tree ring data of Meko et al. (2007) to refine the upper Colorado River flow for the past 1200+ years (Fig. 4e). This comparison is shown in Fig. 4.

In this comparison, it is important to remember that although a northward avulsion is more likely to occur during flood conditions in a wet year, the base-level changes involved would favor rapid headward-cutting and enlargement of the channel in the alluvial terrain, as observed in 1905–1907, and the entire flow of the Colorado River would eventually be captured (Waters, 1983), even if an extended and severe drought immediately followed the flood that initially triggered the avulsion. In other words, even if an avulsion is more likely to occur during a wet period, much of the lake filling and the entirety of the highstand are no more likely to occur during a wet period than during a dry period.

While there are more high discharge events in the upper Colorado River flow reconstruction (Robeson et al., 2020) than there are lakes in the Salton Basin, we can look to (approximate) overlap between the two (Fig. 4) to propose discrete intervals that are more likely to have triggered the lake filling. The middle of the window for the Lake F highstand corresponds to a period of elevated river flow (blue rectangles above Lake F trapezoids in Fig. 4c and d) and, if this is when Lake F actually began filling, it would agree with the notion that lake fillings should initiate during wet periods. In the base model, the Lake E highstand post-dates a brief wet period at ~1000 CE (Fig. 4c), while the alternative model moves the timing of Lake E back by two decades (Fig. 4d); considering the 13–20 years required to fill Lake Cahuilla (Rockwell et al., 2018), the avulsion may have indeed occurred during the period of high flow at ~1000 CE (blue rectangles above Lake E trapezoids in Fig. 4c and d). The base model places most of Lake D in the longest drought of the past millennium, though Lake D may have initiated filling during the preceding wet period at ~1110 CE (blue rectangle above Lake D trapezoid in Fig. 4c); alternatively, Model 2 shifts the middle of Lake D forward into an extended wet period at ~1200 CE, which would be another likely candidate for the timing of the avulsion that led to Lake D (blue rectangle above Lake D trapezoid in Fig. 4d). For Lake D, we cannot strictly distinguish between these two possibilities with data presently available, though the later wet interval (1179–1221 CE) is arguably a more likely candidate for the avulsion that led to the filling of Lake D, as it was the longer and wetter interval (Fig. 4e). The ages of Lakes A, B, and C all overlap with wet periods (blue rectangles above Lakes A, B, and C trapezoids in Fig. 4c and d), consistent with avulsions of the Colorado River northward into the Salton Basin occurring during periods of elevated rainfall and river flow.

As stated in the previous section, because we cannot know whether the alternative model is more defensible than the base

Fig. 5. Changes from the base model (Model 1; a, c, e) to the alternative model (Model 2; b, d, f), as indicated by the dashed boxes. The main difference in Model 2 is that ten PDFs appear in purple, indicating that they were excluded a priori in Model 2, either to test the sensitivity of the OxCal model to the sparse sampling from Lake G or to test its sensitivity to isolated samples that do not necessarily date a dry period between lakes. In Model 1 the youngest date in the dry period before Lake D (Sb4m26A-c) was removed a posteriori as an outlier (a), but in Model 2 the a priori removal of the two oldest dates in the dry period before Lake C (Sb3m4B-b-hum and T2-Sb2-4-c) results in the inclusion of Sb4m26A-c, which was not flagged as an outlier in Model 2 (b). Similarly, in Model 1 the oldest date in the dry period before Lake D (Sb4m49B-b-AAA) was removed a posteriori as an outlier (c), but in Model 2 the a priori removal of the two youngest dates in the dry period before Lake E (IFD-T4-C412 and Sb3m7A-c) results in the inclusion of Sb4m49B-b-AAA, which was not flagged as an outlier in Model 2 (d). Finally, in Model 1 the youngest date in the dry period before Lake G (IFD-T4-C394b) was removed a posteriori as an outlier (e), but in Model 2 the a priori removal of the six oldest dates in the dry period before Lake F results in the inclusion of IFD-T4-C394b, which was not flagged as an outlier in Model 2 (f). The effects of these changes are seen in Fig. 4. See Supplementary Figs. S21–S26 and Supplementary Table S1 for full details of each model. (For interpretation of the references to colour in this figure legend, the reader is referred to the Web version of this article.)

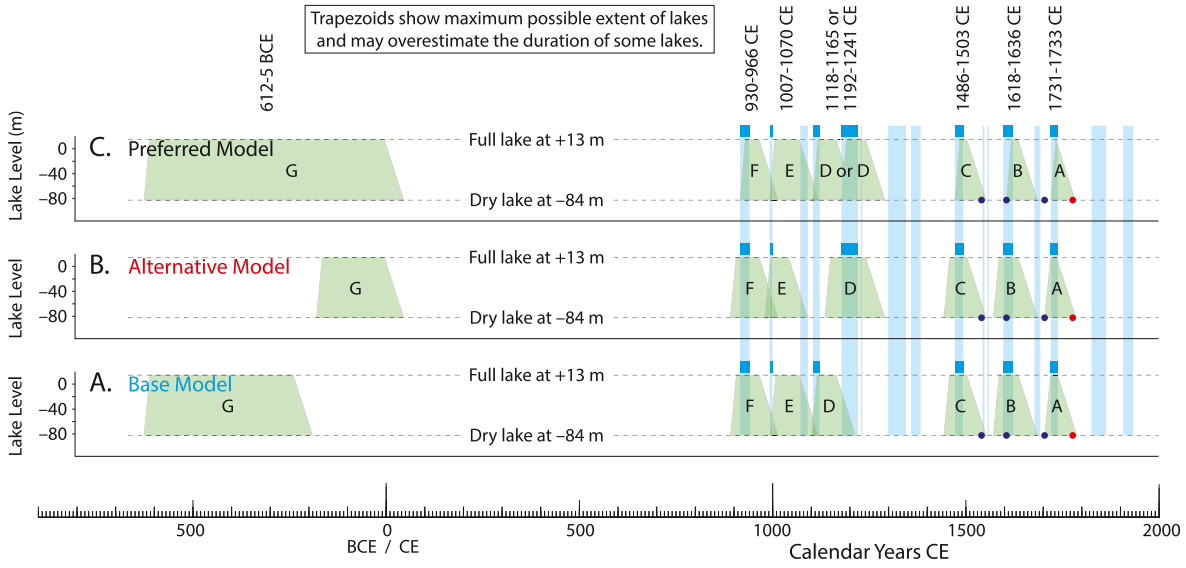

Fig. 6. Preferred Lake Cahuilla chronology. Initially, for each lake highstand, the full range of possible dates is considered, allowing for uncertainties in either (a) the base model or (b) the alternative model. In (c), the preferred model, the full range of possible dates is then trimmed based on historical observations and a streamflow reconstruction. This trimming includes delaying the onset of each lake so that the earliest possible initiating of filling (lower left corner of each trapezoid) aligns with the beginning of the wet period (left side of the corresponding blue rectangle). Trapezoids show maximum possible extent of lakes; the actual timing and extent of a given lake could be anywhere within the respective trapezoid. The years shown above the trapezoids in (c) represent the maximum allowable window for each lake highstand. Symbology follows from Fig. 4. (For interpretation of the references to colour in this figure legend, the reader is referred to the Web version of this article.)

model, any differences between the two models should be considered indicative of real uncertainty in the lake ages. Our preferred model age for each lake should therefore span the respective uncertainties from the base and alternative models. Additionally, if we wish to consider the streamflow reconstruction as a guide to potential timings of northward avulsions of the Colorado River that are more plausible, then we would not expect any lake to begin filling earlier than the blue rectangles above the respective trapezoids in Fig. 4c and d. In our preferred model (Fig. 6c), we combine the uncertainties for each lake from the base and alternative models (Fig. 6a–b, respectively), but we delay the onset of each lake so that the earliest possible initiating of filling (lower left corner of each trapezoid) corresponds to the onset of the wet period (left side of the corresponding blue rectangle).

For Lakes A, B, C, and F the preferred model closely resembles the base and alternative models, but for Lakes E and G the possible window for each lake is expanded relative to the corresponding extent in the base or alternative models individually. For Lake D, two plausible windows emerge, depending upon whether the lake began filling during the wet period around 1110 CE or during the longer wet period around 1200 CE (Fig. 6). The two possible windows in the preferred model for Lake D, and the broader possible ranges for Lakes E and G, result from ambiguity over the validity of the assumptions underpinning the alternative model. These broader windows do not imply that those lakes were necessarily longer-lived than other lakes, but it suggests that additional dates are needed to better constrain the timing of those lakes.

The base and alternative models suggest the Lake B highstand most likely occurred sometime between 1587 and 1636 CE (Fig. 4). Considering the 13–20 years required to fill Lake Cahuilla (Rockwell et al., 2018), this implies that the filling started between 1567 and 1623 CE. Additional information comes from the historical observations of Oñate and Escobar, who described the Colorado River flowing to the Gulf of California in 1605 (purple dot in Lake B in Fig. 4c and d; Rockwell et al., 2018). These details collectively suggest one of two scenarios: either Lake B filled mostly in the late 16th century and the Colorado River had reverted to southward flow into the Gulf of California by 1605, or the avulsion leading to Lake B occurred only after 1605. A comparison to the streamflow reconstruction (Fig. 4) reveals that in the former scenario, the Lake B filling would have necessarily initiated during an extended dry period in the late 16th century. In contrast, in the latter scenario, the filling would have initiated during the "early 1600s pluvial" of Robeson et al. (2020). Based on the streamflow reconstruction and historical data, we consider a post-1605 avulsion to be more likely, which implies that a full Lake B could not have occurred earlier than 1618. This tightens the age of the Lake B highstand in the preferred model to between 1618 and 1636 CE (Fig. 6c).

For Lake A, Anza's inability to find water during treks across the Salton Basin in 1774–1776 suggests that Lake A must have begun desiccating no later than ~1733 CE (Rockwell et al., 2018). As discussed by Rockwell et al. (2018), the filling of Lake A may have initiated during several comparatively wet years beginning in ~1718; if so, the Lake A highstand may have lasted only a few years (Fig. 6c).

It is notable that Ross (2020) argues that the avulsion that occurred in 1905, and which resulted in the Salton Sea, was a natural event and would have occurred separately from human interventions. This avulsion also occurred during a wet period in the Colorado River basin, termed the "early 1900s pluvial" by Robeson et al. (2020), and followed several years of low rainfall. As rainfall remained high for the following two decades, Ross (2020) argues that without human intervention, it is possible that the basin could have filled once again.

The above notwithstanding, it is important to emphasize that, unlike most lakes, Lake Cahuilla is not necessarily high during long wet periods and low during long dry periods. This occurs because the timing of avulsions of the Colorado River is likely controlled by single floods in individual wet years, but the beginning of the highstand would necessarily lag behind the avulsion by 13–20 years and may extend into a drought. To illustrate the uniqueness of the paleohydrologic setting of Lake Cahuilla, we note that a number of pluvial lakes filled basins within the Mojave Desert in the late Pleistocene, but these lakes gradually receded and transitioned to

playa conditions as the climate became more arid in the early Holocene. In some locations, such as at Soda Lake, wetland conditions briefly returned at the time of the Medieval Climate Anomaly and Little Ice Age, but otherwise the past 9 ka have been generally dry (Honke et al., 2019). In contrast, conditions in the Salton Basin have changed rapidly and frequently, with six unique lake fillings and desiccations alone between the 10th and 18th centuries CE.

Given the dynamics of Lake Cahuilla paleohydrology, we do not expect a correlation between regional paleoclimate and the timing of Lake Cahuilla highstands, beyond the potential correlation between Colorado River streamflow, Colorado River avulsions, and the initiation of filling of Lake Cahuilla. Additionally, climate histories have not necessarily been consistent across the region. For instance, Meko et al. (2007) identified the extended drought in the upper Colorado River Basin in the mid-1100s which coincided with dry conditions in the Great Basin, but they concluded that it did not coincide with droughts elsewhere in the American West.

Finally, the comparison of the OxCal models with the streamflow reconstruction reveals that some significant wet periods are clearly not associated with lake highstands, such as the two extended periods of high rainfall between 1300 and 1400 CE, between Lakes D and C (Fig. 4). While this conclusion seems inescapable, we note that water does spill into the basin from time to time, more frequently than full avulsions. For instance, water was observed flowing into the Salton Basin historically in 1840, 1842 or 1849 (accounts differ), 1852, 1859, 1862, 1867, 1884, and 1891 (Orcutt, 1891; Barrows, 1900; Cory, 1913, pp. 1228, 1247; Sykes, 1914, p. 19; MacDougal, 1915, pp. 234–235), though none of these instances led to a full Lake Cahuilla.

Although in our preferred model we delayed the onset of each lake so that the earliest possible initiation of filling aligns with the beginning of the corresponding wet period, these shifts in the lake timings were no more than a few decades in any case (compare Figs. 4 and 6): the beginning of the Lake B highstand was pushed forward by 31 years; the beginning of the Lake C highstand was pushed forward by 27 years; and the beginning of the Lake F highstand was pushed forward by 23–24 years; for other lakes, the shift was 12 years or less.

5.3. Highstand elevation for each lake

Deposits from Lakes A, B, and C are observed and dated at multiple +13 m shoreline sites (Supplementary Table S1), but Lakes D, E, and F left unambiguous, conformable deposits only at sites at 8–9 m above sea level (e.g., Coachella and Carrizo Wash) or lower. Of Lakes D, E, and F, two of them left deposits at +13 m at the SMF Northern Shoreline site, but it is unclear which two they are, and it is unclear whether evidence for the third lake was simply cut out by fluvial erosion or if one of the lakes did not quite make it up to +13 m (Supplementary Text S1 §3.5; Supplementary Fig. S19). In any case, at least five of the past six lakes must have reached the +13 m shoreline. So far, unambiguous, conformable deposits from a seventh lake (Lake G) have been found and dated only at the Imperial fault site at −32 m, although deposits from this lake are likely observed below local unconformities at sites much higher in the basin, perhaps up to 13 m above sea level (Supplementary Text S1; Supplementary Figs. S8, S9, S20; Supplementary Table S1).

Based on the evidence, it is likely that all seven lakes reached at least +9 m, and at least five of the lakes, including with certainty the past three, reached +13 m. It is unlikely that any lake rose higher than +13 m, as this is the modern elevation of the sill of the Colorado River delta, i.e., the minimum crest altitude of the delta at Cerro Prieto (Waters, 1983). Once the lake reached this level, any additional input into Lake Cahuilla would be balanced by southward overflow across the delta into the Gulf of California.

5.4. Evidence for the completeness of desiccations between highstands

To get at the question of whether there was complete desiccation between each highstand, we consider how many discrete lakes are observed at sites at different elevations in the basin, but we must also consider the possibility for a partial filling of the basin that is seen only at the lower-elevation sites. There is compelling evidence from sites at or near the shoreline for six lake highstands (A–F) in the past 1100 years. Many of these sites also record an earlier lake highstand (G) that is capped by a pronounced oxidation horizon or soil, suggesting there was a long gap in deposition between Lakes F and G; however, the only useful dating constraints on Lake G come from lower in the basin (Table 1). Rockwell et al. (2011) document all seven of these lakes at the Dogwood paleoseismic site, so we know that each of the lakes desiccated to at least −32 m elevation. Using the desiccation rate range of 1.52–2.05 m/yr (Rockwell et al., 2018), this 45 m drop in water level would have required 22–30 years. Further, there is evidence at the Salt Creek paleoseismic site, which lies at −60 m, for the presence of at least five and possibly as many as seven discrete lakes, but not necessarily with intervening dry periods, in the past 1100 years (Williams and Seitz, 2005), although the presence of root casts between some lakes does indicate desiccation down to at least −60 m. A seventh lake in the past 1100 years could have resulted from a partial filling of the basin, as occurred in 1905–1907 when the Salton Sea formed: the water reached the Salt Creek site in that filling and flooded Salt Creek up to −59.6 m (Sieh and Williams, 1990). If all six of the Lake Cahuilla highstands in the past 1100 years desiccated to as low as −60 m, this 73 m drop in lake level would have required at least 48–67 years between successive highstands, using the desiccation rates and filling model of Rockwell et al. (2018). This could be consistent with the preferred model (Fig. 6c), as long as Lake F began desiccating by 940–959 CE. Wood growth within the lake footprint may not only span the entire period between successive highstands, but it would start in different locations once the lake level dropped below a site's elevation and would continue until that elevation was re-inundated.

5.5. Archeological and seismological considerations

The more precise timing of past lakes helps to refine, and perhaps even resolve, a number of research problems. For one, this new chronology will permit a more robust comparison between archaeology or imprecisely dated oral traditions with more accurately dated historical information. Our models constrain when the Indigenous Americans occupied shoreline sites for fishing, versus when lake-bottom farming occurred (Wilke, 1978). Arrangement of fish traps at various elevations below the highstand shoreline indicate that they seasonally rebuilt new traps to account for the drawdown of the lake (Phukan et al., 2019) until the water became too saline, resulting in major fish die-offs (Wilke, 1978). Historical accounts record that the Indigenous Cahuilla farmed the lakebed southeast of Palm Springs during the contact period (Blake, 1915), and that there was an oral tradition of fishing the lake in the past.

Additionally, many paleoseismic studies have been completed around the lake basin, from sites at the highstand shoreline (Sieh, 1986; Sieh and Williams, 1990; Pollard and Rockwell, 1995; Gurrola and Rockwell, 1996; Faneros, 2005) to other sites close to or above sea level (Thomas and Rockwell, 1996; Orgil, 2001; Ragona, 2003; Philibosian et al., 2011; Jerrett, 2015; Wessel, 2015), to sites well below sea level (Williams, 1989; Sieh and Williams, 1990; Meltzner et al., 2006; Rockwell et al., 2011). Many of these have limited radiocarbon control, but all reference the timing of earthquakes relative to various Lake Cahuilla highstands. The ages of the

interpreted earthquakes recorded at these various sites can be recalculated with these new lake age data such that large earthquakes in the southern San Andreas system can be sequenced to test whether rupture patterns of triggering emerge.

5.6. Age inheritance in radiocarbon dates

As noted previously, 120 of the 284 stratigraphically well-defined dates in our compilation (42%) are out of sequence and clearly older than a stratigraphically lower lake, demonstrating significant age inheritance beyond the calibrated age uncertainty; some samples date thousands of years older than the inferred sediment age. This number (120 of 284) is likely an undercount, as dates with some overlap with the bulk of the younger ages for each lake were retained, yet these may nonetheless have some degree of inheritance. Considered another way, at flatter parts of the radiocarbon calibration curve, high-precision dates with an age inheritance of ~150 years could easily have been missed in our count, but the same amount of age inheritance would have been obvious (and statistically significant) at a steeper part of the calibration curve.

Furthermore, the in situ mesquite stumps capped by Lake A deposits provide robust evidence that the lakebed was dry and that Lake A did not fill until sometime after 1705 CE. Nevertheless, 21 of the 51 radiocarbon samples within deltaic, lacustrine, or shoreline deposits associated with Lake A (41%) are necessarily older than 1705 CE, i.e., none of those samples' age PDFs overlap with 1705 CE at 95% confidence. Notably, eight of these samples (16%) are too old by > 600 years, and five of these samples (10%) are too old by > 1000 years.

Collectively, these observations imply that statistically significant age inheritance should be expected in more than 40% of all radiocarbon samples in the Salton Basin, with the inherited age (the difference between the sample age and the age of the sediment it is collected from) exceeding 1000 years ~10% of the time.

Nonetheless, it is also remarkable that for each of Lakes A, B, and C, at least 15 dates from sites scattered around the basin give indistinguishable and reliable ages for the dry period immediately preceding the respective lake (Fig. 3). As we have shown, the age clustering can be used to overcome the age inheritance problem, as long as rational, defensible age models are constructed with those clustered radiocarbon dates.

6. Conclusions

To constrain the timing of the past seven lake highstands in the Salton Trough, we compiled 423 radiocarbon dates, of which 284 are reliable and have good stratigraphic control. We developed two models in OxCal, a base model and an alternative model, which use 151 and 149 of the dates, respectively, after discarding dates that are out of sequence (indicating age inheritance) or that were flagged by OxCal for having poor agreement. Notably, 120 of the 284 reliable dates were rejected because they clearly violated stratigraphic ordering, implying that more than 40% of all radiocarbon dates in the Salton Basin exhibit statistically significant age inheritance.

The radiocarbon dates and Bayesian modeling in OxCal cannot by themselves distinguish between the base and alternative models (Fig. 4); the differences in the models result from choices of whether to include or exclude specific dates that may or may not be representative of a particular dry period. Where the base and alternative models are similar, the results can be considered robust, but where the models differ, any differences between the two models should be considered a reflection of the true uncertainty in the lake ages. Consideration of historical accounts and a high-resolution paleohydrologic reconstruction allows us to trim the ages of Lakes A and B, and the paleohydrologic reconstruction also provides insight into the most likely intervals during which earlier lakes may have initiated filling.

The preferred model age windows for the past seven Lake Cahuilla highstands are 1731–1733 CE (Lake A), 1618–1636 CE (Lake B), 1486–1503 CE (Lake C), 1118–1165 or 1192–1241 CE (Lake D), 1007–1070 CE (Lake E), 930–966 CE (Lake F), and 612–5 BCE (Lake G). These ages represent the maximum allowable ranges during which a lake may have filled the basin up to the +13 m highstand elevation; the basin may have been dry for a significant portion of each time window. Additionally, the Colorado River avulsion that initiated each filling likely occurred 13–20 years prior to the beginning of the respective highstand, and a complete desiccation would have required at least 47 years after the end of the highstand (Rockwell et al., 2018); the lake filling and desiccation episodes may have extended beyond the aforementioned highstand age range for each lake. If the paleohydrologic constraints are ignored, some of the lakes may have initiated earlier, by up to three decades.

Author Contributions

Thomas K. Rockwell: Conceptualization, Methodology, Formal analysis, Investigation, Writing – original draft, Writing – review & editing, Visualization, **Aron J. Meltzner:** Methodology, Formal analysis, Investigation, Data curation, Writing – original draft, Writing – review & editing, Visualization, **Erik C. Haaker**: Methodology, Investigation, Writing – review & editing, **Danielle Madugo**: Investigation, Writing – review & editing

Declaration of competing interest

The authors declare that they have no known competing financial interests or personal relationships that could have appeared to influence the work reported in this paper.

Acknowledgements

We thank the many researchers who have worked on Lake Cahuilla and with whom we have had numerous discussions over the years, including but not limited to Jerry Schaefer, Belle Philibosian, Ray Weldon, Kate Scharer, Kerry Sieh, Gordon Seitz, and Pat Williams. We thank Kate Scharer, Pat Williams, and an anonymous reviewer for thoughtful, constructive feedback on an early version, which substantially improved the manuscript. We also thank Glenn Biasi and Joanne Lim for insight, suggestions, and assistance with probabilistic calculations. This research was supported by the Southern California Earthquake Center (SCEC Contribution # 10218). SCEC is funded by NSF Cooperative Agreement EAR-1600087 & USGS Cooperative Agreement G17AC00047. This research was also funded by the National Research Foundation Singapore and the Singapore Ministry of Education under the Research Centres of Excellence initiative. This is Earth Observatory of Singapore Contribution Number 318.

Appendix A. Supplementary data

Supplementary data to this article can be found online at https://doi.org/10.1016/j.quascirev.2022.107456.

References

Anderson, L., Zentner, E., Nagy, V., Hagan, C., Thompson, R., Kidwell, K., Salinas, H., 2022. California Wildfire History Map. Capital Public Radio. https://projects.capradio.org/california-fire-history/.

Arkush, B.S., 1990. Archaeological Investigations at CA-RIV-1182, CA-RIV-3143, CA-RIV-3144, CA-RIV-3868, and CA-RIV-3882, Tentative Tract 25429, La Quinta,

Central Riverside County, California. Archaeological Research Unit, University of California, Riverside.
Aschmann, H., 1959. The evolution of a wild landscape and its persistence in Southern California. Ann. Assoc. Am. Geogr. 49 (No. 3, Part 2), 34–56. https://www.jstor.org/stable/2561246.
Barrows, D.P., 1900. The Colorado Desert. Natl. Geogr. Mag. 11, 337–351.
Blake, W.P., 1915. Sketch of the region at the head of the Gulf of California. In: Cory, H.T. (Ed.), The Imperial Valley and the Salton Sink. J.J. Newbegin, San Francisco, California, pp. 1–35. https://archive.org/details/imperialvalleya00blakgoog.
Blong, R., Gillespie, R., 1978. Fluvially transported charcoal gives erroneous ^{14}C ages for recent deposits. Nature 271, 739–741. https://doi.org/10.1038/271739a0.
Bronk Ramsey, C., 1995. Radiocarbon calibration and analysis of stratigraphy: the OxCal program. Radiocarbon 37, 425–430. https://doi.org/10.1017/S0033822200030903.
Bronk Ramsey, C., 2008. Deposition models for chronological records. Quat. Sci. Rev. 27, 42–60. https://doi.org/10.1016/j.quascirev.2007.01.019.
Bronk Ramsey, C., 2009a. Bayesian analysis of radiocarbon dates. Radiocarbon 51, 337–360. https://doi.org/10.1017/S0033822200033865.
Bronk Ramsey, C., 2009b. Dealing with outliers and offsets in radiocarbon dating. Radiocarbon 51, 1023–1045. https://doi.org/10.1017/S0033822200034093.
Brothers, D.S., Driscoll, N.W., Kent, G.M., Harding, A.J., Babcock, J.M., Baskin, R.L., 2009. Tectonic evolution of the Salton Sea inferred from seismic reflection data. Nat. Geosci. 2, 581–584. https://doi.org/10.1038/ngeo590.
Brothers, D., Kilb, D., Luttrell, K., Driscoll, N., Kent, G., 2011. Loading of the San Andreas fault by flood-induced rupture of faults beneath the Salton Sea. Nat. Geosci. 4, 486–492. https://doi.org/10.1038/ngeo1184.
Cory, H.T., 1913. Irrigation and river control in the Colorado River delta. Trans. Am. Soc. Civ. Eng. 76, 1204–1453 paper no. 1270. https://doi.org/10.1061/TACEAT.0002448. Reprinted in Cory, H.T., 1915. The Imperial Valley and the Salton Sink, J.J. Newbegin, San Francisco, California, 452 pp. https://archive.org/details/imperialvalleya00blakgoog.
Erlandson, J.M., Rockwell, T.K., 1987. Radiocarbon reversals and stratigraphic discontinuities: the effects of natural formation processes on coastal California archeological sites. In: Nash, D.T., Petraglia, M.D. (Eds.), Natural Formation Processes and the Archaeological Record. British Archaeological Reports International Series 352, pp. 51–73.
Faneros, G.A., 2005. Structure and Neotectonics of the Superstition Mountain Fault, Imperial County, California. MS Thesis. San Diego State University. http://hdl.handle.net/20.500.11929/sdsu:26237.
Fletcher, J.M., Teran, O.J., Rockwell, T.K., Oskin, M.E., Hudnut, K.W., Mueller, K.J., Spelz, R.M., Akciz, S.O., Masana, E., Faneros, G., Fielding, E.J., Leprince, S., Morelan, A.E., Stock, J., Lynch, D.K., Elliott, A.J., Gold, P., Liu-Zeng, J., González-Ortega, A., Hinojosa-Corona, A., González-García, J., 2014. Assembly of a large earthquake from a complex fault system: surface rupture kinematics of the 4 April 2010 El Mayor–Cucapah (Mexico) M_w 7.2 earthquake. Geosphere 10, 797–827. https://doi.org/10.1130/GES00933.1.
Gavin, D., 2001. Estimation of inbuilt age in radiocarbon ages of soil charcoal for fire history studies. Radiocarbon 43, 27–44. https://doi.org/10.1017/S003382220003160X.
Gurrola, L.D., Rockwell, T.K., 1996. Timing and slip for prehistoric earthquakes on the Superstition Mountain fault, Imperial Valley, southern California. J. Geophys. Res. 101, 5977–5985. https://doi.org/10.1029/95JB03061.
Haaker, E.C., 2012. Moving towards a More Complete Late Holocene Chronology of Ancient Lake Cahuilla. BS Thesis. San Diego State University.
Honke, J.S., Pigati, J.S., Wilson, J., Bright, J., Goldstein, H.L., Skipp, G.L., Reheis, M.C., Havens, J.C., 2019. Late Quaternary paleohydrology of desert wetlands and pluvial lakes in the Soda Lake basin, central Mojave Desert, California (USA). Quat. Sci. Rev. 216, 89–106. https://doi.org/10.1016/j.quascirev.2019.05.021.
Jerrett, A.S., 2015. Paleoseismology of the Imperial Fault at the US–Mexico Border and Correlation of Regional Lake Stratigraphy through Analysis of Oxygen/Carbon Isotope Data. MS Thesis. San Diego State University. http://hdl.handle.net/20.500.11929/sdsu:1764.
Laylander, D., 1997. The last days of Lake Cahuilla: the Elmore site. Pacific Coast Archaeological Society Quarterly 33, 1–138. http://www.pcas.org/V3312.htm.
Li, H.-C., You, C.-F., Ku, T.-L., Xu, X.-M., Buchheim, H.P., Wan, N.-J., Wang, R.-M., Shen, M.-L., 2008. Isotopic and geochemical evidence of palaeoclimate changes in Salton Basin, California, during the past 20 kyr: 2. $^{87}Sr/^{86}Sr$ ratio in lake tufa as an indicator of connection between Colorado River and Salton Basin. Palaeogeogr. Palaeoclimatol. Palaeoecol. 259, 198–212. https://doi.org/10.1016/j.palaeo.2007.10.007.
MacDougal, D.T., 1915. The Salton Sea. Am. J. Sci. (4th series) 39, 231–250. https://doi.org/10.2475/ajs.s4-39.231.231.
Meko, D., Woodhouse, C.A., Baisan, C.A., Knight, T., Lukas, J.J., Hughes, M.K., Salzer, M.W., 2007. Medieval drought in the upper Colorado River basin. Geophys. Res. Lett. 34, L10705. https://doi.org/10.1029/2007GL029988.
Meltzner, A.J., 2006. Characterization of the Long-Term Behavior of the Imperial and Brawley Faults, Imperial Valley, California. MS Thesis. San Diego State University. http://hdl.handle.net/20.500.11929/sdsu:26314.
Meltzner, A.J., Rockwell, T.K., Owen, L.A., 2006. Recent and long-term behavior of the Brawley fault zone, Imperial Valley, California: an escalation in slip rate? Bull. Seismol. Soc. Am. 96, 2304–2328. https://doi.org/10.1785/0120050233.
Modesto, R., Mount, G., 1980. Not for Innocent Ears: Spiritual Traditions of a Desert Cahuilla Medicine Woman. Sweetlight Books, Arcata, California, p. 120.
Monitoring Trends in Burn Severity (MTBS), 2022. Interactive Viewer. United States Department of Agriculture (Forest Service) / U.S. Geological Survey. https://mtbs.gov/viewer/.
Orcutt, C.R., 1891. A visit to Lake Maquata. The West American Scientist 7, 158–164. https://archive.org/details/westamericanscie759orcut.
Orgil, A., 2001. Three-dimensional Paleoseismic Investigation on the South Break of the Coyote Creek Fault, Southern California. MS Thesis. San Diego State University. http://hdl.handle.net/20.500.11929/sdsu:26337.
Philibosian, B., Fumal, T., Weldon, R., 2011. San Andreas fault earthquake chronology and Lake Cahuilla history at Coachella, California. Bull. Seismol. Soc. Am. 101, 13–38. https://doi.org/10.1785/0120100050.
Phukan, A., Braje, T.J., Rockwell, T.K., Ullah, I., 2019. Shorelines in the desert: mapping fish trap features along the southwest coast of ancient Lake Cahuilla, California. Advances in Archaeological Practice 7, 325–336. https://doi.org/10.1017/aap.2019.31.
Pollard, W.J., Rockwell, T.K., 1995. Late Holocene slip rate for the Coyote Creek fault, Imperial County, California. Abstr. Progr. Geol. Soc. Am. 27 (5), 72.
Ragona, D., 2003. A High-Resolution Paleoseismic Study in the Southern San Jacinto Fault Zone, Imperial County, California. MS Thesis. San Diego State University. http://hdl.handle.net/20.500.11929/sdsu:28066.
Reimer, P., Austin, W., Bard, E., Bayliss, A., Blackwell, P., Bronk Ramsey, C., Butzin, M., Cheng, H., Edwards, R., Friedrich, M., Grootes, P., Guilderson, T., Hajdas, I., Heaton, T., Hogg, A., Hughen, K., Kromer, B., Manning, S., Muscheler, R., Palmer, J., Pearson, C., van der Plicht, J., Reimer, R., Richards, D., Scott, E., Southon, J., Turney, C., Wacker, L., Adolphi, F., Büntgen, U., Capano, M., Fahrni, S., Fogtmann-Schulz, A., Friedrich, R., Köhler, P., Kudsk, S., Miyake, F., Olsen, J., Reinig, F., Sakamoto, M., Sookdeo, A., Talamo, S., 2020. The IntCal20 Northern Hemisphere radiocarbon age calibration curve (0–55 cal kBP). Radiocarbon 62, 725–757. https://doi.org/10.1017/RDC.2020.41.
Robeson, S.M., Maxwell, J.T., Ficklin, D.L., 2020. Bias correction of paleoclimatic reconstructions: a new look at 1,200+ years of Upper Colorado River flow. Geophys. Res. Lett. 47, e2019GL086689. https://doi.org/10.1029/2019GL086689.
Rockwell, T.K., Meltzner, A., Tsang, R., 2011. A Long Record of Earthquakes with Timing and Displacements for the Imperial Fault: a Test of Earthquake Recurrence Models. Final Technical Report. U.S. Geological Survey, 28 pp.
Rockwell, T.K., Fletcher, J.M., Teran, O.J., Hernandez, A.P., Mueller, K.J., Salisbury, J.B., Akciz, S.O., Štěpančíková, P., 2015. Reassessment of the 1892 Laguna Salada earthquake: fault kinematics and rupture patterns. Bull. Seismol. Soc. Am. 105, 2885–2893. https://doi.org/10.1785/0120140274.
Rockwell, T.K., Meltzner, A.J., Haaker, E.C., 2018. Dates of the two most recent surface ruptures on the southernmost San Andreas Fault recalculated by precise dating of Lake Cahuilla dry periods. Bull. Seismol. Soc. Am. 108, 2634–2649. https://doi.org/10.1785/0120170392.
Ross, J.E., 2020. Formation of California's Salton Sea in 1905–07 was not "accidental". In: Miller, D.M. (Ed.), Changing Facies: the 2020 Desert Symposium Field Guide and Proceedings. Desert Symposium, Inc., Zzyzx, CA, pp. 217–230. http://www.desertsymposium.org/History.html.
Schaefer, J., 1987. The Ormesa-IID Transmission Line and Ormesa Geothermal Pipeline Network Cultural Resources Survey and Testing Program, East Mesa, Imperial County, California. Mooney-Levine and Associates, San Diego, California.
Schaefer, J., Pallette, D., 1993. Archaeological Investigations of Two Lake Cahuilla Sites in the Toro Canyon Area, Riverside County, California. Brian F. Mooney Associates, San Diego, California.
Schiffer, M.B., 1986. Radiocarbon dating and the "old wood" problem: the case of the Hohokam chronology. J. Archaeol. Sci. 13, 13–30. https://doi.org/10.1016/0305-4403(86)90024-5.
Sieh, K.E., 1986. Slip rate across the San Andreas and prehistoric earthquakes at Indio, California. Eos Trans. Am. Geophys. Union 67, 1200.
Sieh, K.E., Williams, P.L., 1990. Behavior of the southernmost San Andreas fault during the past 300 years. J. Geophys. Res. 95, 6629–6645. https://doi.org/10.1029/JB095iB05p06629.
Slingerland, R., Smith, N.D., 2004. River avulsions and their deposits. Annu. Rev. Earth Planet. Sci. 32, 257–285. https://doi.org/10.1146/annurev.earth.32.101802.120201.
Sykes, G., 1914. Geographical features of the Cahuilla Basin. In: MacDougal, D.T. (Ed.), The Salton Sea: a Study of the Geography, the Geology, the Floristics, and the Ecology of a Desert Basin. Carnegie Institution of Washington, Washington, D.C., pp. 13–20. https://archive.org/details/saltonseastudyof00macduoft. https://archive.org/details/cu31924002078065
Sykes, G., 1937. The Colorado Delta. Carnegie Institution of Washington Publication 460 and American Geographical Society Special Publication 19, Washington, D.C. https://catalog.hathitrust.org/Record/001631435.
Thomas, A.P., Rockwell, T.K., 1996. A 300- to 550-year history of slip on the Imperial fault near the U.S.–Mexico border: missing slip at the Imperial fault bottleneck. J. Geophys. Res. 101, 5987–5997. https://doi.org/10.1029/95JB01547.
U.S. Geological Survey and California Geological Survey, 2020. Quaternary Fault and Fold Database of the United States. Updated 2 September 2020. https://www.usgs.gov/natural-hazards/earthquake-hazards/faults.
Verdugo, D., 2004. Further Resolution of Past Earthquake Surface Ruptures at Carrizo Wash, Southern San Jacinto Fault, Imperial Valley, California: the Devil is in the Deposits. BS Thesis. San Diego State University. http://hdl.handle.net/20.500.11929/sdsu:30450.
Waters, M.R., 1983. Late Holocene lacustrine chronology and archaeology of ancient Lake Cahuilla, California. Quat. Res. 19, 373–387. https://doi.org/10.1016/0033-5894(83)90042-X.

Weide, D.L., 1974. Regional environmental history of the Yuha Desert region. In: Weide, M.L., Barker, J.P., Lawton, H.W., Weide, D.L., Wilke, P.J. (Eds.), Background to Prehistory of the Yuha Desert Region. Report for U.S. Department of Interior, Bureau of Land Management, California Desert Planning Program, pp. 4–15. https://doi.org/10.6067/XCV8X34WNH.

Wessel, K.N., 2015. 500 Year Rupture History of the Imperial Fault at the International Border through Analysis of Faulted Lake Cahuilla Sediments, Carbon-14 Data, and Climate Data. MS Thesis. San Diego State University. http://hdl.handle.net/20.500.11929/sdsu:1832.

Wilke, P.J., 1978. Late Prehistoric Human Ecology at Lake Cahuilla, Coachella Valley, California. Contributions of the University of California Archaeological Research Facility. Department of Anthropology, University of California Berkeley, No. 38, 168 pp. https://escholarship.org/uc/item/8367m039.

Williams, P.L., 1989. Aspects of the Earthquake Geology and Seismotectonics of the Southern San Andreas and Related Faults, Southern California. Ph.D. Thesis. Columbia University, New York, New York.

Williams, P., Seitz, G., 2005. Development of Earthquake Slip and Age Constraints, Southernmost San Andreas Fault, California. Final Technical Report. USDI/USGS Awards 04HQGR0003 and 04HQGR0012, 6 pp.

Williams, P., Seitz, G., 2006. New insights to earthquake behavior of the southernmost San Andreas fault. Seismol. Res. Lett. 77, 270. https://doi.org/10.1785/gssrl.77.2.160.

White, E.M., 2017. Determining Radiocarbon Reservoir Corrections for Freshwater Mollusks from Ancient Lake Cahuilla, Imperial County, California. MS Thesis. San Diego State University. http://hdl.handle.net/20.500.11929/sdsu:21608.

Yohe II, R.M., 1990. Archaeological Investigations at Five Sites Located at One Eleven La Quinta Center in the City of La Quinta, Central Riverside County, California. Archaeological Research Unit, University of California, Riverside.